OPEN ACCESS

African Journal of **Biotechnology**

March 2021
ISSN 1684-5315
DOI: 10.5897/AJB
www.academicjournals.org

ACADEMIC JOURNALS
expand your knowledge

About AJB

The African Journal of Biotechnology (AJB) is a peer reviewed journal which commenced publication in 2002. AJB publishes articles from all areas of biotechnology including medical and pharmaceutical biotechnology, molecular diagnostics, applied biochemistry, industrial microbiology, molecular biology, bioinformatics, genomics and proteomics, transcriptomics and genome editing, food and agricultural technologies, and metabolic engineering. Manuscripts on economic and ethical issues relating to biotechnology research are also considered.

Indexing

CAB Abstracts, CABI's Global Health Database, Chemical Abstracts (CAS Source Index) Dimensions Database, Google Scholar, Matrix of Information for The Analysis of Journals (MIAR), Microsoft Academic, Research Gate

Open Access Policy

Open Access is a publication model that enables the dissemination of research articles to the global community without restriction through the internet. All articles published under open access can be accessed by anyone with internet connection.

The African Journals of Biotechnology is an Open Access journal. Abstracts and full texts of all articles published in this journal are freely accessible to everyone immediately after publication without any form of restriction.

Article License

All articles published by African Journal of Biotechnology are licensed under the Creative Commons Attribution 4.0 International License. This permits anyone to copy, redistribute, remix, transmit and adapt the work provided the original work and source is appropriately cited. Citation should include the article DOI. The article license is displayed on the abstract page the following statement:

This article is published under the terms of the Creative Commons Attribution License 4.0
Please refer to https://creativecommons.org/licenses/by/4.0/legalcode for details
about Creative Commons Attribution License 4.0

Memberships and Standards

Academic Journals strongly supports the Open Access initiative. Abstracts and full texts of all articles published by Academic Journals are freely accessible to everyone immediately after publication.

All articles published by Academic Journals are licensed under the Creative Commons Attribution 4.0 International License (CC BY 4.0). This permits anyone to copy, redistribute, remix, transmit and adapt the work provided the original work and source is appropriately cited.

Crossref is an association of scholarly publishers that developed Digital Object Identification (DOI) system for the unique identification published materials. Academic Journals is a member of Crossref and uses the DOI system. All articles published by Academic Journals are issued DOI.

Similarity Check powered by iThenticate is an initiative started by CrossRef to help its members actively engage in efforts to prevent scholarly and professional plagiarism. Academic Journals is a member of Similarity Check.

CrossRef Cited-by Linking (formerly Forward Linking) is a service that allows you to discover how your publications are being cited and to incorporate that information into your online publication platform. Academic Journals is a member of CrossRef Cited-by.

Academic Journals is a member of the International Digital Publishing Forum (IDPF). The IDPF is the global trade and standards organization dedicated to the development and promotion of electronic publishing and content consumption.

Contact

Editorial Office: ajb@academicjournals.org

Help Desk: helpdesk@academicjournals.org

Website: http://www.academicjournals.org/journal/AJB

Submit manuscript online http://ms.academicjournals.org

Academic Journals
73023 Victoria Island, Lagos, Nigeria
ICEA Building, 17th Floor,
Kenyatta Avenue, Nairobi, Kenya.

Editor-in-Chief

Editorial Board Members

Table of Content

Vol. 20(3), pp.108-114, March, 2021
DOI: 10.5897/AJB2020.17246
Article Number: 2F0F6ED66193
ISSN: 1684-5315

http://www.academicjournals.org/AJB

ACADEMIC JOURNALS
expand your knowledge

African Journal of Biotechnology

Full Length Research Paper

Comparison of homogenization methods for extraction of maize cob metabolites

Jeremy Winders[1]* and Tibor Pechan[2]

[1]Chemistry Research Unit, Center for Medical, Agricultural and Veterinary Entomology, Department of Agriculture, Agricultural Research Service, Gainesville, FL, 32608, USA.
[2]Institute for Genomics, Biocomputing and Biotechnology, Mississippi State University, Mississippi State, USA.

Received 16 September, 2020; Accepted 21 January, 2021

Previous proteomic studies have shown maize cob tissue to have an essential role in pathogen defense. Currently, there are no studies published regarding neither maize cob metabolomic profiles nor an accepted method of metabolite extraction from cob. This study assesses the reproducibility of metabolite extraction from the cobs of fungal pathogen -resistant and -susceptible cultivars. Hand grinding, mechanical ball-milling and adapted focused acoustics methods of tissue homogenization were preformed and examined via Liquid Chromatography-Mass Spectrometry (LC-MS). Among tested methods, the manual grinding with a mortar and pestle was found to be the most reproducible and efficient. All methods showed good reproducibility within but provided statistically different sets of metabolite features when compared across methods. A suitable extraction method for future cob metabolomics experiments was ascertained, however careful results validation will be needed to distinguish between true biological phenomenon and artifacts rising from a methodology bias. For the first time, maize cob metabolites have been successfully extracted and detected, establishing a reproducible method for further metabolomic profiling of cob defense metabolites.

Key words: Liquid Chromatography-Mass Spectrometry (LC-MS), metabolomics, *Aspergillus flavus,* homogenization, extraction, grinding.

INTRODUCTION

In maize (*Zea mays* L.), the cob provides mechanical support to kernels in addition to transporting essential nutrients and water. Previous studies have shown that cob tissue plays an essential role in both facilitating and limiting the spread of the fungal pathogen *Aspergillus flavus* which causes ear rot and produces the carcinogenetic metabolite aflatoxin B1 (Alfaro, 2000; Magbanua et al., 2013). Previous proteomic analysis of cob tissue revealed the presence of constitutive and fungal-induced defense proteins (Pechanova and Pechan, 2015; Pechanova et al., 2011), suggesting defense metabolites in the parent cob tissue are linked to the defense response in the developing kernel. To date, no metabolomic profiling studies for cob have been published

*Corresponding author. E-mail: jeremy.winders@usda.gov.

in the literature. This study provides the initial step towards a maize cob global metabolomic profiling study by establishing the impacts of different types of tissue disruption and homogenization on the reproducibility of features detected in metabolomics analysis via Liquid Chromatography-Mass Spectrometry (LC-MS).

Unlike soft tissues of maize, cob is very rigid and presents a challenge as it ages and becomes hardened. Compared to kernel or leaf tissues, cob requires an extensive force to be ground into the fine powder needed for metabolite extraction. No protocol for extraction of metabolites from maize cob tissue has been established in the literature. It has been previously shown that sample preparation and extraction of plant tissues impact the reproducibility of metabolites detected via LC-MS (de Souza et al., 2019; Kim and Verpoorte, 2010; Tugizimana et al., 2018). Thus, this study investigates the reproducibility and efficiency of metabolite extractions from maize cob using three different grinding techniques as an initial step. Methods differ by modes of tissue homogenization, manual grinding, mechanical cryo-grinding, and tissue disruption via Adaptive Focused Acoustic (AFA) technology; but are identical during metabolite elution phase. Mortar and pestle are commonly used for grinding soft tissues into a powder but is labor-intensive and not well suited for callous tissue. The ball mill grinder offers a fast, automated approach to homogenization. The Covaris S220 acoustic focused-ultrasonicator (AFA) was chosen because of its effective cellular disruption previously observed in proteomics.

The *A. flavus* resistant Mp313E (Scott and Zummo, 1990) and susceptible B73 (Russell, 1972) maize cultivars were chosen as study subjects, due to their availability and connection to previous proteomic studies (Pechanova et al., 2011). Metabolites from three technical replicates for both cultivars were extracted using three different grinding methods and subjected to LC-MS analysis. Raw data files were processed by the Sieve software (ThermoFisher Scientific, Waltham, MA). The Principal Component Analysis (PCA) showed the similarities and differences between genotypes, replicates, and extraction methods. Venn diagrams were created to evaluate method efficiency via detection of unique and overlapping features produced by the three grinding methods for both genotypes.

MATERIALS AND METHODS

Metabolite extraction methods

Since metabolites are in flux within a plant system, extreme care was taken to minimize perturbation and/or degradation. Maize plants were field grown in a randomized complete block design with 20 plants per row at Mississippi State University R. R. Foil Plant Science Research Center. Inbreeds were matched as per maturity for each genotype by harvesting ears at 33 days after mid-silk (at least 50 % of the plants in the block had silk showing in the primary ear).

The healthy primary maize ears were harvested from the stalk and were immediately placed on ice during transportation from the field to the laboratory. All kernels, silks, and piths were removed from the cob and a 3.5 cm section of cob was harvested above and below the centermost point. The cob section was then sliced into 1 mm thick disks before being diced. The chopped cob tissue was then flash-frozen in liquid nitrogen, to minimize metabolites degradation (Jones and Kinghorn, 2006), and stored at -80°C until extraction. Six biological replicate tissue samples from each genotype were pooled and split into three technical replicates. When weighing samples, the tubes of stock tissue were removed from cold storage and placed into a liquid nitrogen bath before and after aliquots were measured. Metabolites were extracted by the previously published protocol (Kim and Verpoorte, 2010) but diverse in modes of tissue homogenization. Cob tissue was disrupted to release metabolites by: 1. manual grinding with a mortar and pestle; 2. mechanical grinding; and 3. Adapted Focused Acoustics technology.

Manual grinding (MG)

Diced cob sample (1.5 g) was placed in a nitrogen chilled mortar. The rigid tissue was vigorously ground by a nitrogen chilled pestle for 8-10 min until only a fine powder was obtained. A paper towel was fitted around the pestle to prevent sample loss through ejection while grinding. Liquid nitrogen was added as needed to mortar to prevent thawing of the tissue.

Mechanical cryogrinding (GG)

Diced cob samples (1.5 g) were ground simultaneously in cycles of 2 min at 200 strokes/min using Spex Sample Prep Geno/Grinder 2000 (SPEX, Metuchen, NJ). Each sample was placed in a 15 ml ball-grinder tube containing three 9.525 mm stainless steel grinding balls (OPS Diagnostics, Lebanon, NJ) that were treated by the manufacturer to remove residual oils and contaminants. The tubes, balls, and stainless steel six-tube rack were pre-chilled in liquid nitrogen before sample insertion. Sample tubes and steel tube rack were kept in a nitrogen bath for 5 min before and after each grinding cycle to reduce tissue thawing. A total of ten cycles were performed, at which point most of the tissue had become a fine powder. Increasing the number of cycles did not improve pulverization any further.

Adapted focused acoustics (AFA)

According to manufacturer protocol for solid samples, diced cob tissue (1.5 g) was inserted into specialized pulverization bags (Cat. No. 520001, Covaris, Woburn, MA), submerged to liquid nitrogen for 1 min, then positioned under an anvil mechanism and hit three times with a mallet, crushing the tissue. The bags were returned to a liquid nitrogen bath for 5 min before being transferred to a specialized AFA vial (Cat. No. 520080, Covaris, Woburn, MA). The sample vial was then placed in a Covaris S220 acoustic focused-ultrasonicator (Covaris, Woburn, MA) that subjected the tissue to 1,000 cycles per burst of 500 W ultrasonic power at a duty factor of 20 over a 1 min period at 4°C to further disrupt the cellular structure of the tissue. The given setup represents the most stringent one allowed by the instrument.

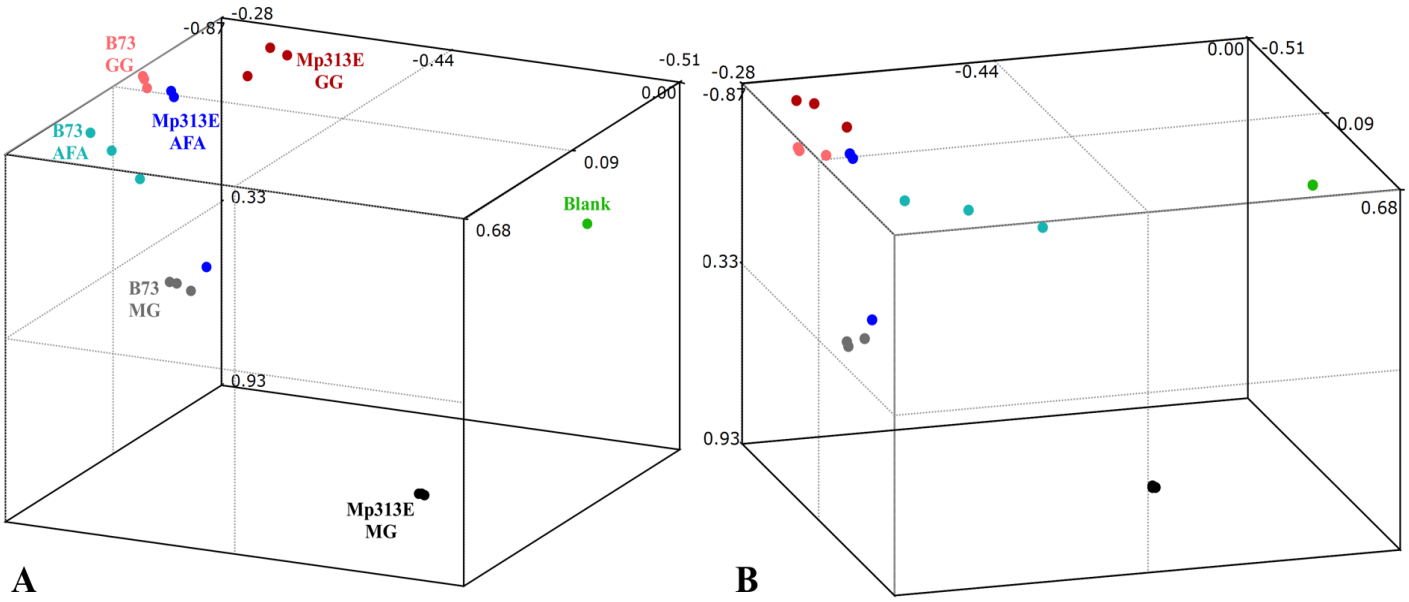

Figure 1. The Principal Component Analysis (PCA) of features/metabolites extracted from cobs of *A. flavus* resistant and susceptible maize genotypes. Each dot represents an individual technical replicate (three replicates were analyzed). Green dots (three overlapping replicates) depict blanks from the extraction buffer. The darker and lighter shades indicate samples from resistant (Mp313E) and susceptible (B73) genotypes, respectively. Black/gray, red/orange, and blue/light blue dots relate to MG, GG, and AFA extraction methods, respectively. (**A**) and (**B**) depict a 3-D PCA from different vantage points. PC1, PC2, and PC3 component scores are labeled on each axis. Additional 3-D rotational views and 2-D PCAs can be found in the supplementary data Figure S1 and S2, respectively.

Chemical elution of metabolites

For all three grinding methods, once the tissue sample had become a fine powder, it was suspended in 4.5 ml of methanol with 0.125% formic acid (v/v) and processed according to Kim and Verpoorte (2010). The suspension was vortexed and then placed in a Cole-Parmer ultra-sonicator (Cole-Parmer, Vernon Hills, IL) bath at 40 kHz for 10 min. Suspensions were centrifuged at 21,130 *x g* for 50 min at 4°C. The supernatant of 3 ml was removed without disturbing the pellet and filtered through a 0.2-micron polytetrafluoroethylene (PTFE) disk syringe filter, and the pellet was discarded. Post filtration, the samples were centrifuged at 21,130 *x g* for 15 min at 4°C to ensure no precipitate remained. The supernatant was transferred to 1.5 ml tubes in aliquots (150 µl) while being speed-vac dried at room temperature. Blank replicates (extraction buffer only) were subjected to the same procedure as the tissue containing samples.

Liquid chromatography–mass spectrometry analysis (LC-MS)

All samples were resuspended in 50 µl of 2% acetonitrile with 0.1% formic acid (v/v). They were analyzed by an Ultimate 3000 HPLC system directly linked to a LTQ Orbitrap Velos mass spectrometer (both ThermoFisher Scientific, Waltham, MA). Seven µl of each sample were loaded on C18 reversed-phase column, and metabolites were separated via constant flow (0.33 µl.min^{-1}), 60-min long linear gradient of acetonitrile in 0.3% formic acid (2% for 5 min, 2 - 75% for 30 min, 95% for 10 min, 2% for 15 min). Analytes were nebulized via nano-electrospray ionization, and mass spectra were collected in full scan, profile, no fragmentation, positive mode, with the mass resolution set to 100,000.

RESULTS AND DISCUSSION

Principal component analysis of metabolite features

To evaluate methods for extractions of metabolites, it is not necessary to actually identify the compounds. The immediate subjects of following analyses are “features” and their intensities as representative parameters of pertinent metabolites entities. The term “feature” describes an LC-MS signal consisting of retention time (RT) and mass to charge ratio (*m/z*) (Tautenhahn et al., 2008). Raw LC-MS data files were analyzed by Sieve software (ThermoFisher Scientific, Waltham, MA) using the “Small molecule chromatographic alignment” module capable of performing principal component analysis (PCA) (Figure 1). Critical processing parameters were set as follows: *m/z* interval 85-900, RT interval 10-50 min., peak time width of 2 min., *m/z* width 7 ppm, the maximum number of frames 3,000, and alignment minimal intensity 1000.

The PCA analysis results show that grouping of detected features was method-dependent, as demonstrated by the clustering of replicates for each extraction technique, rather than clustering based on genotypes. As indicated by the tight clustering of the manual ground (MG) Mp313E (black dots) and MG B73 replicates (gray dots), manual grinding showed the

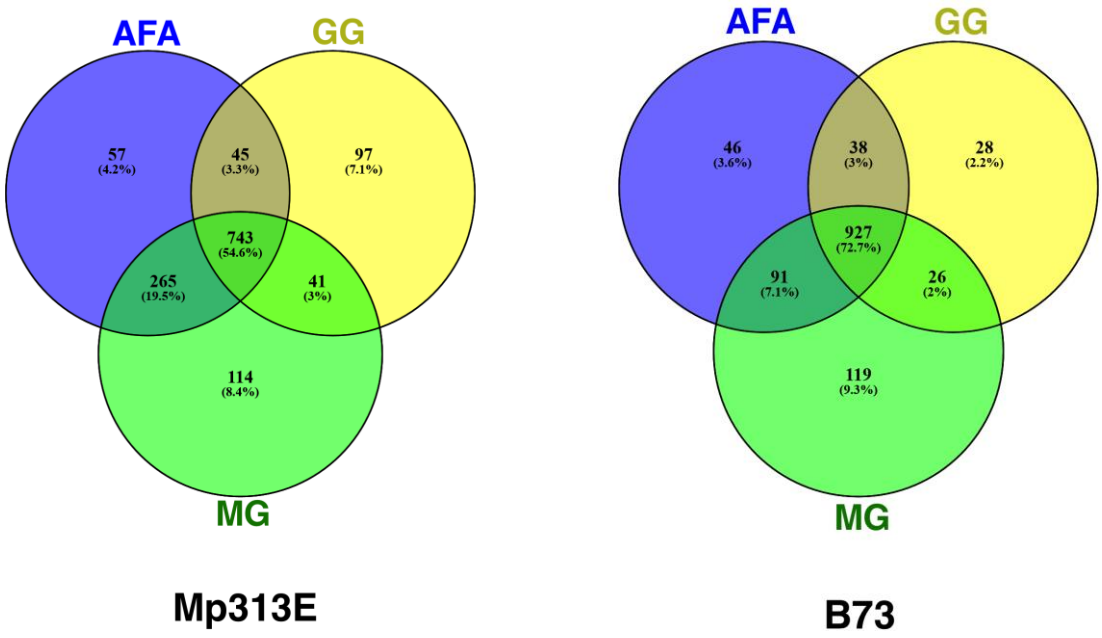

Figure 2. The Mp313E and B73 Venn diagrams show the overlapping and method-unique features produced by each of the three extraction methods: Adapted Focused Acoustics (AFA), mechanical grinding (GG), or manual grinding (MG).

highest reproducibility among tested methods. The second-best reproducibility was achieved by the mechanical grinding method (GG), where both GG Mp313E (red dots) and GG B73 (orange dots) exhibited close clustering of replicates. Most loosely grouped replicates were the Adaptive Focused Acoustics (AFA) Mp313E (blue dots) and B73 (light blue dots), indicating that the Adaptive Focused Acoustics method of homogenization is the least reproducible. The three Blank replicates (green dots) overlap and appear as a single dot in PCA from any angle, affirming high reproducibility of LC-MS data collection. Therefore, observed differences among the replicates across the methods can be confidently attributed to true differences in extracted metabolomes, rather than to irreproducible LC-MS measurements.

Venn diagrams of unique and overlapping metabolite features

The features detected by Sieve software for each method and genotype were exported to Venny online software software (BioinfoGP Madrid, Spain) (Oliveros, 2007-2015) to create strict Venn diagrams (Figure 2). The number of features detected in Mp313E samples obtained via AFA, GG, and MG method was 1,102; 1,019; and 1,163 respectively, for a total of 1,362. In B73 genotype, respective numbers were 1,110; 926; and 1163, totaling 1,275 features. There was 54.6% and 72.7% overlap among all three methods for Mp313E and B73 genotype, respectively. The manual grinding produced the highest number of method-unique features (8.4% and 9.3% of the total features detected in Mp313E and B73, respectively). The differences among methods in regard to total and unique features are quite small (~ 21% and 9%, respectively, in most extreme cases), but nevertheless, the results point to MG as the most efficient method.

DISCUSSION

Interestingly, the most primitive method of tissue homogenization, manual grinding (MG), has proven to be the most reproducible and efficient, out of the three tested techniques for maize cob homogenization and single solvent metabolite extraction. It is possible that MG technique dominates “because of”, and not “despite” being a purely manual, human-controlled method. Unlike the “robotic” methods, MG allows for intelligent intervention for the finest grinding via the ability to see and target the remaining larger pieces of cob tissue to achieve a more homogeneous powder sample. Contrary to expectation, mechanical grinding (GG) commonly left small pieces (1 mm in diameter) of intact cob tissue in the ball-grinder tube, regardless of a prolonged time of processing or increasing the number of balls. Similarly, the temperature can be controlled more consistently

during manual grinding, as spontaneous additions of liquid nitrogen in response to thawing. During mechanical grinding, nitrogen cooling of utilized hardware occurred before and after each of the pulverization cycles. Local heating due to friction between balls and tissue could have occurred to the level promoting random molecule degradation, affecting the reproducibility and efficiency of the method. The Adapted Focused Acoustics (AFA) method yields were slightly better than for mechanical grinding. Obviously, the sonic bursts are powerful enough to release small molecules from hard cob tissue. However, the reproducibility was lowest, possibly due to random movement of the cob particles within sonication vials, and due to uncontrolled metabolites reactions taking place at a comparatively high temperature (4°C) during tissue disruption.

Conclusion

This study explored a critical initial step in a larger scope metabolomics experiment – single solvent extraction of metabolites from a tissue of interest, particularly the maize cob, which has not been scrutinized yet for its role in molecular defense against pathogens. Three grinding techniques were examined and quantified in regard to their reproducibility, efficiency, and general feature detection for later LC-MSn experiments. Out of those three, the best performing extraction method for future cob metabolomics experiments was ascertained, however careful results validation will be needed to distinguish between true biological phenomenon and artifacts rising from a methodology bias. Future cob metabolite extractions will combine manual and mechanical grinding aspects to maximize feature extraction, reproducibility, and physical effort as the number of samples scales up.

CONFLICT OF INTERESTS

The authors have not declared any conflict of interests.

ACKNOWLEDGEMENTS

We thank Dr. Olga Pechanova for her help and guidance in early stages of the project. This work was supported by Genomics of Agricultural Species and their Pest and Pathogens (USDA Award No. 58-6066-6-04) and the National Institute of Food and Agriculture's Agriculture and Food Research Initiative for Education and Literacy Initiative (Award No. 2017-67011-26081). Additionally, the USDA-ARS Corn Host Plant Resistance Research Unit at Mississippi State University supported field work and sample collection.

REFERENCES

Alfaro Y (2000). Response of resistant and susceptible maize genotypes to inoculation with transformed Aspergillus flavus isolates. https://elibrary.ru/item.asp?id=5476413

de Souza LP, Alseekh S, Naake T, Fernie A (2019). Mass Spectrometry-Based Untargeted Plant Metabolomics. Current Protocols in Plant Biology 4(4):e20100. doi:10.1002/cppb.20100.

Jones WP, Kinghorn AD (2006). Extraction of plant secondary metabolites. Natural Products Isolation 323-351 https://link.springer.com/protocol/10.1385/1-59259-955-9:323

Kim HK, Verpoorte R (2010). Sample preparation for plant metabolomics. Phytochemical Analysis 21(1): 4-13.

Magbanua ZV, Williams WP, Luthe DS (2013). The maize rachis affects Aspergillus flavus spread during ear development. Maydica 58(2):182-188.

Oliveros JC (2007-2015). An interactive tool for comparing lists with Venn's diagrams. https://bioinfogp.cnb.csic.es/tools/venny/

Pechanova O, Pechan T (2015). Maize-pathogen interactions: an ongoing combat from a proteomics perspective. International Journal of Molecular Sciences. 16(12): 28429-28448.

Pechanova O, Pechan T, Williams WP, Luthe DS (2011). Proteomic analysis of the maize rachis: potential roles of constitutive and induced proteins in resistance to Aspergillus flavus infection and aflatoxin accumulation. Proteomics 11(1): 114-127.

Russell W (1972). Registration of B70 and B73 Parental Lines of Maize1 (Reg. Nos. PL16 and PL17). Crop Science 12(5): 721-721.

Scott GE, Zummo N (1990). Registration of Mp313E parental line of maize. Crop Science 30(6):1378-1378

Tautenhahn R, Boettcher C, Neumann S (2008). Highly sensitive feature detection for high resolution LC/MS. BMC Bioinformatics 9(1): 504.

Tugizimana F, Steenkamp PA, Piater LA, Dubery IA (2018). Mass spectrometry in untargeted liquid chromatography/mass spectrometry metabolomics: Electrospray ionisation parameters and global coverage of the metabolome. Rapid Communications in Mass Spectrometry 32(2): 121-132.

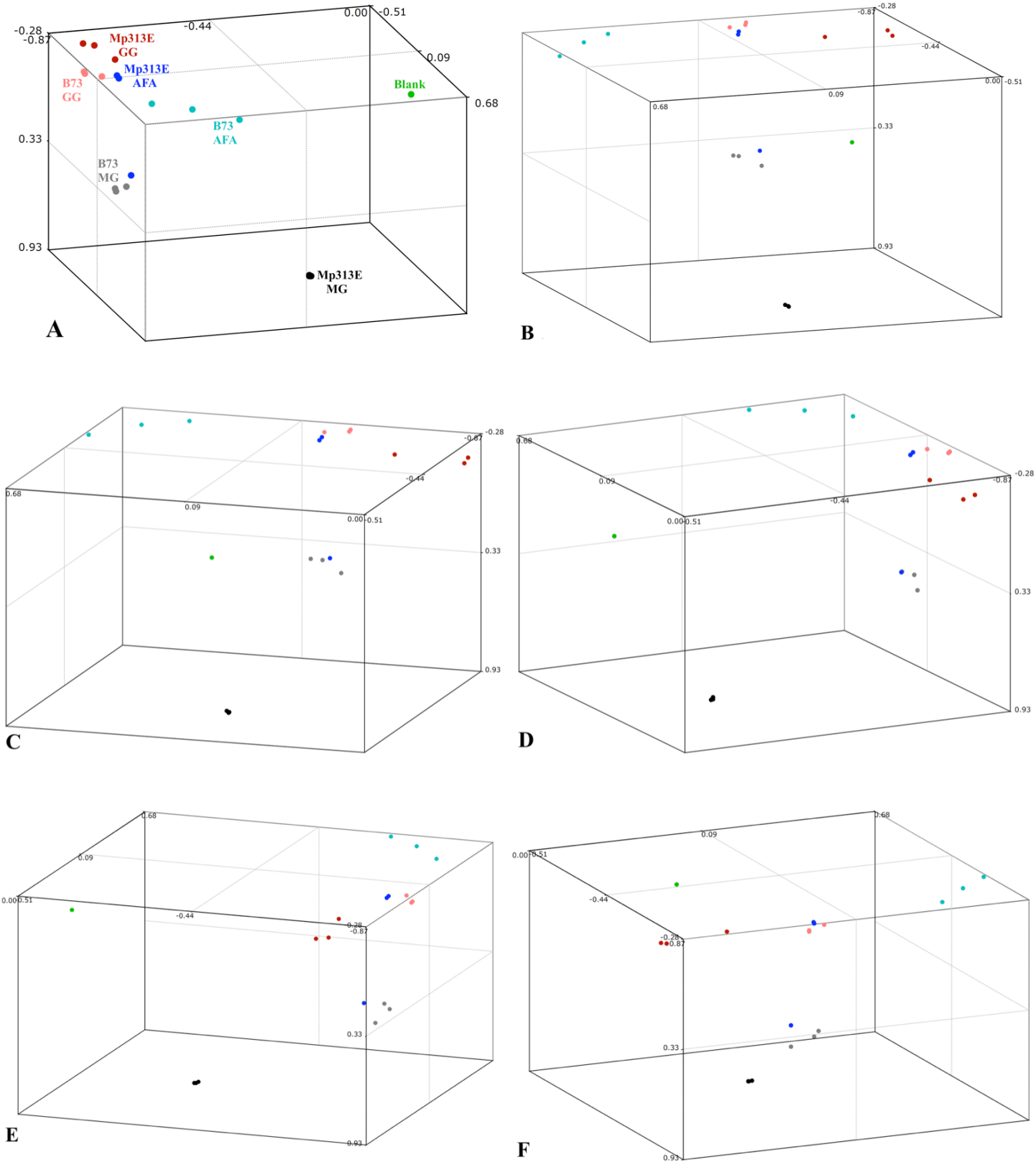
-0.28
-0.87
-0.44
0.00
-0.51
0.09
0.68
0.33
0.93
Mp313E
GG
Mp313E
AFA
B73
GG
B73
AFA
B73
MG
Blank
Mp313E
MG
A
B
C
D
E
F

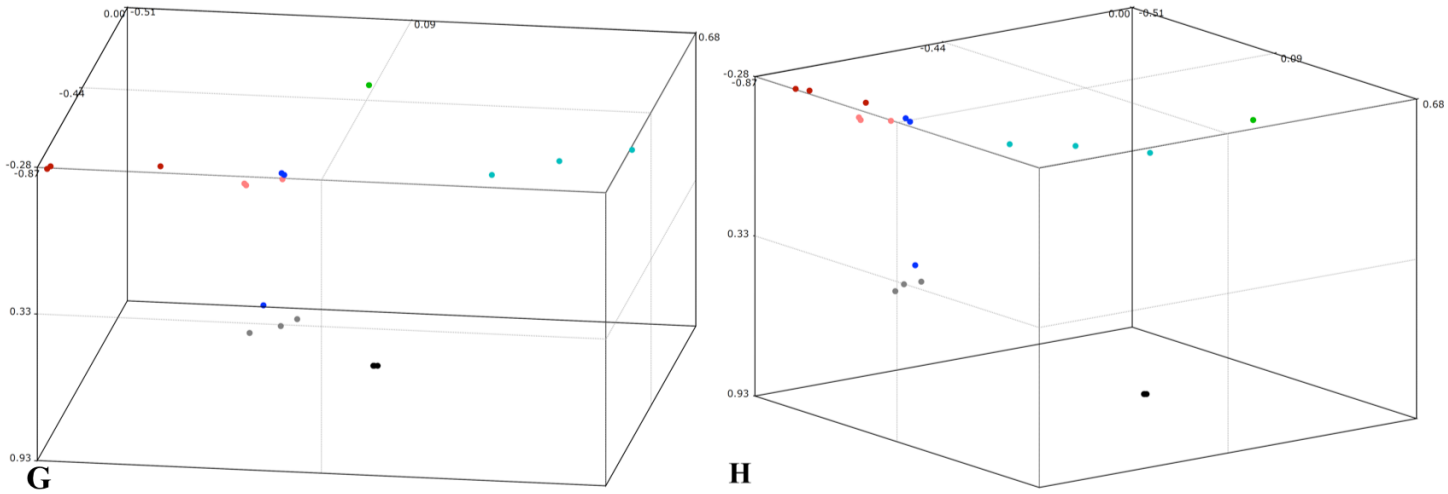

Figure S1. The Principal Component Analysis (PCA) of features/metabolites extracted from cobs of *A. flavus* resistant and susceptible maize genotypes. Each dot represents an individual technical replicate (three replicates were analyzed). Green dots (they overlap) depict blanks). The darker and lighter shades indicate samples from resistant (Mp313E) and susceptible (B73) genotypes, respectively. Black/gray, red/orange, and blue/light blue dots relate to MG, GG and AFA extraction methods, respectively. (**A**-**H**) depict 3-D PCA image from different vantage points (rotated left).

Vol. 20(3), pp.115-121, March, 2021
DOI: 10.5897/AJB2020.17242
Article Number: B5AA5FD66312
ISSN: 1684-5315

http://www.academicjournals.org/AJB

ACADEMIC JOURNALS
expand your knowledge

African Journal of Biotechnology

Full Length Research Paper

Brewer's residues and cocoa pod shells as a substrate for cultivation of *Pleurotus ostreatus* CCIBt 2339 and enzymes production

Carolina Fernandes Pereira[1], Antônio Zózimo de Matos Costa[2], Givaldo Rocha Niella[2], José Luiz Bezerra[3], Ana Paula Trovatti Uetanabaro[1] and Elizama Aguiar-Oliveira[1*]

[1]Universidade Estadual de Santa Cruz (UESC), Rodovia Jorge Amado, km 16, Salobrinho, CEP: 45.662-900, Ilhéus, Bahia, Brazil.
[2]Comissão Executiva do Plano da Lavoura Cacaueira (CEPLAC), Centro de Pesquisas do Cacau, Seção de Fitopatologia. Rodovia Jorge Amado, km 22, CEP: 45.600-000, Itabuna, Bahia, Brazil.
[3]Universidade Federal do Recôncavo da Bahia (UFRB), Centro de Ciências Agrárias, Ambientais e Biológicas. Campus de Cruz das Almas, CEP: 44.380-000, Cruz das Almas, Bahia, Brazil.

Received 12 September, 2020; Accepted 6 October, 2020

This work investigated the best composition of a substrate for cultivation of *Pleurotus ostreatus* CCIBt 2339 using brewer's spent grain (SG) and cocoa pod shells (CP) complemented with hot trub (HT) and/or residual brewer's yeast (RY). The residue HT was detrimental for cultivation and a substrate composition (%, w/w) of 58% *SG* + 40% *CP* + 2% *RY* – with a C/N ratio of 25.77 g/g – resulted in the best values of biological efficiency (*BE* = 1.204.0 g/kg) and productivity [*Pd* = 32.5 g/(kg.day)]. The crude multi-enzymatic extract, obtained as a result of the mycelial growth in this substrate was a good source for: laccases (7.644.4 U/g), xylanases (110.9 U/g) and amylases (277.4 U/g). The obtained results demonstrate the biotechnological potential for the proposed substrate for edible mushrooms production as much as for the obtaining of enzymes with industrial application.

Key words: Carbon/Nitrogen ratio, cellulases, pectinase, simplex-centroid design, tannase.

INTRODUCTION

Mushrooms are excellent natural agents for degradation of lignocellulosic compounds besides all of their nutritional and/or medicinal value (Stamets, 2005). A good example of versatility and efficiency, is the edible mushroom *Pleurotus ostreatus*, which is a basidiomycete highly appreciated in different countries and has been cultivated on a wide variety of vegetable-based substrates (Ergun and Urek, 2017; Silva et al., 2019). Considering the current context when it is necessary to promote the valorization of different residues for different purposes, four agro-industrial residues generated from the production lines of beer [brewer's spent grain (SG), hot trub (HT) and residual brewer's yeast (RY)] and chocolate [cocoa pod husks (CP)] were selected as

*Corresponding author. E-mail: elizamaguiar@yahoo.com.br.

potential substrates for cultivation of edible mushrooms.

The two main residues selected, SG and CP, can be considered good sources of carbon. In general, SG contains around 530 g/kg of polysaccharides and 100 g/kg of lignin (Hassan et al., 2020; Rojas-Camorro et al., 2020), while CP can contain from 430 to 490 g/kg of carbon with about 210 g/kg of lignin (Adjin-Tetteh et al., 2018; Antwi et al., 2019). To balance the ratio between carbon and nitrogen, HT and RY were selected, basically due to their protein content. For HT, levels of 200 to 700 g/kg of protein were estimated (Mattioli et al., 2020) and, for RY*,* around 25.3 g/kg of nitrogen (Puligundla et al., 2020). Considering the available data for 2018, over 5 million tons of cocoa beans are produced worldwide (FAOSTAT, 2020) and CP can represent 70 to 75% of the total weight of the fruit (Shet et al., 2018). Additionally, China, United States and Brazil were the three largest beer producers reaching more than 730 million hectoliters in 2018 (STATISTA, 2020) and SG is estimated to be around 85% of the total by-products generated in the beer-brewing process (Hassan et al., 2020). Thus, the four residues proposed, which have a rich nutritional composition, are generated in significant quantities and can be potentially suggested (with low environmental impact) for the production of edible mushrooms. Therefore, this present work investigated the best composition between SG and CP supplemented with HT and/or RY as a substrate for *P. ostreatus* CCIBt 2339 cultivation, and, consequently, to obtain multi-enzymatic extracts.

MATERIALS AND METHODS

Pleurotus ostreatus CCIBt 2339

P. ostreatus CCIBt 2339, originally from the Instituto de Botânica de São Paulo (São Paulo, SP, Brazil), was made available by the Comissão Executiva do Plano da Lavoura Cacaueira (CEPLAC, Itabuna, BA, Brazil). The strain was preserved in penicillin tubes (Castellani, 1967) and maintained in potato-dextrose-agar (PDA). Periodically, cultivation in a bio-oxygen-demand incubator (BOD) (SL-200, SOLAB Científica) was conducted at 25°C in Petri dishes with PDA until complete coverage of the surface by the vegetative mycelium (around 20 days).

Preparation of residues and substrates

Brewer's spent grain (SG), hot trub (HT*)* and residual brewer's yeast (RY) were acquired at the Microbrewery of the Universidade Estadual de Santa Cruz (Ilhéus, BA, Brazil) after a production of a Witbier beer with: wheat and barley malts, cardamom, nutmeg and hop pellets (U.S. Golding Hops). SG was dried in an oven (MA-035, MARCONI) at 60°C until constant weight; HT and RY were autoclaved at 121°C/15 min (CS50, Prismatec), frozen (-80°C/24 h) and dried in a lyophilizer (LS3000, TERRONI). Cocoa pod shells (CP) were obtained from local producers from Ilhéus (Bahia, Brazil) and were manually chopped before drying, as performed for SG, and then crushed to a particle size of 3 to 4 cm. The compositions (g/kg, dry base) of carbon (C) and nitrogen (N), for each residue, were estimated (IAL, 2008); for technical limitations, only humidity (% w/w, dry base) was possible to be determined in triplicate (MB-120, OHAUS). Table 1 presents these compositions which were applied in the calculations of the C/N ratio (g/g) and the amount of water necessary to reach the substrate initial humidity of 70% (w/w).

The substrates were prepared, according to each composition to be evaluated, by weighing the pre-treated residues and mixing them with water. After 1 h, 100 g of substrate were transferred to polypropylene bags (50 × 30 cm), which were closed with an acrylic fabric and rubber bands (to allow aeration) and autoclaved (121°C/20 min) twice within 48 h (Marino and Abreu, 2009; Oliveira et al., 2007).

Spawn preparation

Based on Oliveira et al. (2007) and Shibata and Demiate (2003), with some modifications, the spawn (seeds) were produced using wheat grains purchased from local business (Ilhéus, BA, Brazil); the grains were cooked in boiling water [ratio of 1:2 (kg:L)] for 15 min; the excess water was drained and, after cooling down, 30 g/kg of a mixture [1:4 (w/w)] of $CaCO_2$ (for pH adjustment) and plaster (to prevent particle agglomeration) was added. The wheat grains were transferred to polypropylene bags (50 × 30 cm) until about ⅔ of its volume (200 g), the bags were closed with an acrylic fabric and rubber bands and then autoclaved (121°C/30 min). After cooling down, ¼ of a Petri dish with complete mycelial growth of *P. ostreatus* CCIBt 2339 was inoculated on the surface of the wheat grains and, once closed, the bags were incubated at 25°C for 10 to 15 days (or until complete colonization). A tray with water was placed at the bottom of the BOD in order to maintain a high humidity (80 – 90% w/w) and it was constantly renewed.

Inoculation, mycelium running, fruiting and harvesting

The substrate inoculation proceeded with 10% (w/w) of spawn and incubation (mycelium running) occurred as described for spwan preparation but for 15 to 20 days (or until complete colonization). Only then, the bags were moved to a refrigerator (4°C/24 h) to promote a temperature shock to induce the appearance of the primordia. After that, the plastic bags were removed to expose the substrate blocks which were individually hung with a hook in boxes in the "fruiting room". The room conditions were maintained as 80 to 90% (w/w) of humidity and 23 to 25°C and a direct artificial light was maintained with fluorescent lamps (55 W, G-LIGHT PREMIUM). After a period of around 15 to 20 days, the fully developed fruiting bodies (first flush) were harvested with a slight twist and pull and were weighed (fresh weight) and measured (diameter).

Study of substrate composition

The best compositions for the residues: SP, HT, RY and CP were investigated based on a 3-component Simplex-Centroid design, totaling 10 different runs, with *SP* varying between 10 and 90% (w/w) and *HT* and *RY*, individually, from 0 to 5% (w/w); CP was used to complement the weight to 100 g. Each run from the matrix was performed in triplicate and the statistical analysis was performed considering the individual (and valid) responses. The main responses analyzed were: biological efficiency (*BE*, g/kg) and productivity [*Pd*, g/(kg day)], the secondary responses were: pileus diameter (d_{pil}, cm) and periods (days) of each phase: mycelium running (t_{mr}), appearance of primordia (t_{ap}) and colonization and harvesting (t_{ch}). Two compositions (%, w/w) were selected and performed in triplicate for experimental validation: S5 (50% *SG* + 2.5% *RY* + 47.5% *CP*) and S11 (58% *SG* + 2% *RY* + 40% *CP*).

Table 1. Compositions (g/kg) of carbon (C) and nitrogen (N) and humidity (%, w/w) obtained for brewer's spent grain (SP), hot trub (HT*)*, residual brewer's yeast (RY) and cocoa pod shells (CP).

Residue	C (g/kg)	N (g/kg)	C/N (g/g)*	Humidity (%, w/w)[§]
SG	501.7	25.1	19.99	7.58 ± 2.50
HT	460.5	46.7	9.86	5.00 ± 3.42
RY	497.3	25.3	19.66	3.57 ± 4.88
CP	481.1	10.2	47.17	9.78 ± 3.42

*C/N ratio; [§]Mean value ± standard deviation, from triplicates.

Characterization of mushrooms and cultivation

Biological efficiency (*BE*, g/kg) expresses the relationship between the weight of fresh mushrooms obtained for each kilogram of initial dry substrate and productivity [*Pd*, g/(kg day)] expresses *BE* by the total time of cultivation until harvesting (t_{ch}, days) (Fonseca et al., 2015; Oliveira et al., 2007). The diameters (d_{pil}, cm) of the harvested fruiting bodies were measured using a (millimeter) ruler. Following the order of cultivation phases, the periods (days) of: mycelium running (t_{mr}), appearance of primordia (t_{ap}) and cultivation until harvesting (t_{ch}) were determined.

Obtaining and characterizing the crude multi-enzymatic extract

Four compositions (%, w/w) were selected and prepared in Petri dishes (30 g, triplicate): S5, S11, S1 (90% *SG* + 10% *CP*) and S9 (23.6% *SG* + 0.85% *HT* + 3.35% *RY* + 72.2% *CP*). The mycelial phase was conducted as previously described and the myceliated substrates were macerated with distilled water [ratio of 1:10 (g:mL)] and stirred in a shaker for 1 h (25°C/200 rpm). The solids were separated by vacuum filtration followed by centrifugation at (4,000 *g*/15 min/5°C) and the supernatant was identified as the crude multi-enzymatic extract (CME) which was investigated for the enzymes: laccase, xylanase, CMCase, FPase, amylase, pectinase and tannase. The spectrophotometric methodologies applied for each enzyme were described previously by Ghose and Bisaria (1987), Lu et al. (2013), Sharma et al. (2000), Umsza-Guez et al. (2011) and Vasconcelos et al. (2013) and the enzymatic activities (U) were expressed per gram of initial dry substrate (U/g).

Statistical analysis

The best adjustment of the obtained responses to a mathematical model (linear, quadratic, special cubic) was selected based on the Analysis of Variance (ANOVA) performed with at least 90% of confidence and the Contour Curves were generated with a statistical software (STATISTICA v.8, StatSoft). Also, the Tukey test was applied to compare mean values of specific conditions with 95% of confidence.

RESULTS AND DISCUSSION

Study of the substrate composition

Table 2 presents the Simplex-Centroid matrix, the C/N ratios for each substrate and the mean responses obtained. Some of the replicates performed were disregarded since they did not result in fruiting bodies during the entire period of cultivation (30 - 45 days), while the other replicates of the same condition did. According to the results, higher C/N (between 30 and 39 g/g) were obtained when *CP* > 60% w/w (S2, S3, S6, S8, S9 and S10) (Table 2). The two highest values of *BE* (> 550 g/kg) and *Pd* [> 16 g/(kg.day)] were obtained with the substrates S1 and S5 (Table 2), with S5 presenting the best performance and a more balanced composition between *SG* and *CP* in relation to S1 which, had the highest *SG* content and the lowest C/N among all the substrates.

Based on the ANOVA for the responses *BE* and *Pd* it was possible to adjust quadratic models with *p*-values < 0.05, however, both mathematical models will not be presented because they also resulted in R^2 and R_{adj}^2 not higher than 0.65 and a statistically significant Lack of Adjustment (*p*-value < 0.05). It should be noted that this does not invalidate the study and the Contour Curves were analyzed together with the experimental data in order to make decisions about the compositions, as described in the following.

As *Pd* is calculated from the *BE* value, only the Contour Curve for *Pd* (Figure 1a) will be presented and discussed, since both curves are remarkably similar. The analysis of Figure 1a indicates a narrow range area in which the best results were obtained close to zero for *HT*, above 0.25 for *SG* and below 0.75 for *RY* where S1 and S5 are located (C/N between 21 and 28 g/g).

The results also allowed to identify that the increase in *HT* was detrimental to *Pd*, probably due to astringent compounds (such as tannins) normally found in this residue (Mattioli et al., 2020), which could act as an anti-nutritional factor (Luz et al., 2013). This effect can be observed when comparing runs S4 and S5 (Table 2), both with the same values for *SG* and *CP* and similar C/N, however, S4 contained *HT* and none of its replicates presented primordia. Thus, considering S5, the relationship between the predicted values of *Pd* and the coded components values (Figure 1b) suggests maximum responses around *SG* = 0.7 and *RY* = 0.3 (which are indicated with arrows in Figure 1b). However, this theoretical condition is remarkably close to run S7 (Table 2) which did not presented primordia. Consequently, a new codified composition was selected and identified as S11 (*SG* = 0.60 + *RY* = 0.40, C/N = 25.77 g/g).

Table 2. Substrate composition for *Pleurotus ostreatus* CCIBt 2339 according to a coded Simplex-Centroid matrix for the components: brewer's spent grain (*SG*), hot trub (*HT*) and residual brewer's yeast (*RY*) with cocoa pod shells (*CP*) as a complementary composition (to 100 g); real values (%, w/w) for the components are presented in parentheses and the C/N ratio (g/g) of each substrate is also indicated. The responses were: biological efficiency (*BE*, g/kg), productivity [*Pd*, g/(kg.day)], diameter (d_{pil}, cm) and times (days) for the stages of: mycelium running (t_{mr}), appearance of primordia (t_{ap}) and cultivation and harvest (t_{ch}).

Run	Component			*CP*	C/N	Responses*					
	***SG* (%, w/w)**	***HT* (%, w/w)**	***RY* (%, w/w)**	**(%, w/w)**	**(g/g)**	***EB* (g/kg)**	***Pd* [g/(kg.day)]**	**d_{pil} (cm)**	**t_{mr} (days)**	**t_{ap} (days)**	**t_{ch} (days)**
S1[#]	1 (90.00)	0 (0.00)	0 (0.00)	10.00	21.16	550.70 ± 169.14	16.81 ± 4.11	1.91 ± 0.40	19.0 ± 0.0	2.5 ± 2.1	32.5 ± 2.1
S2[§]	0 (10.00)	1 (5.00)	0 (0.00)	85.00	35.67	227.23 ± 46.39	6.40 ± 1.80	2.63 ± 0.32	22.3 ± 2.3	7.7 ± 0.6	36.3 ± 7.5
S3	0 (10.00)	0 (0.00)	1 (5.00)	85.00	38.89	148.9	3.82	2.21	25	10	39
S4[§]	½ (50.00)	½ (2.50)	0 (0.00)	47.50	26.44	0 ± 0	0 ± 0	0 ± 0	25.0 ± 3.5	0 ± 0	0 ± 0
S5[#]	½ (50.00)	0 (0.00)	½ (2.50)	47.50	27.28	649.80 ± 8.06	19.40 ± 0.17	2.21 ± 0.04	17.0 ± 2.8	4.5 ± 2.1	33.5 ± 0.7
S6[#]	0 (10.00)	½ (2.50)	½ (2.50)	85.00	37.21	211.90 ± 60.81	6.75 ± 2.08	2.19 ± 0.28	19.0 ± 0.0	9.0 ± 0.0	31.5 ± 0.7
S7[§]	⅔ (63.60)	⅙ (0.85)	⅙ (0.85)	34.70	27.55	0 ± 0	0 ± 0	0 ± 0	19 ± 0	0 ± 0	0 ± 0
S8[#]	⅙ (23.60)	⅔ (3.35)	⅙ (0.85)	72.20	32.24	253.35 ± 1.91	5.98 ± 0.54	2.17 ± 0.07	20.0 ± 1.4	7.0 ± 0.0	42.5 ± 3.5
S9[§]	⅙ (23.60)	⅙ (0.85)	⅔ (3.35)	72.20	33.46	320.73 ± 91.65	8.62 ± 1.25	3.42 ± 1.44	21.0 ± 3.5	9.7 ± 3.1	36.7 ± 5.9
S10[#]	⅓ (36.40)	⅓ (1.65)	⅓ (1.65)	60.30	29.65	307.15 ± 25.95	7.68 ± 0.65	2.73 ± 0.56	21.0 ± 0.0	8.5 ± 0.7	40.0 ± 0.0

*Mean values ± standard deviation, from [§]triplicates and [#]duplicates.

According to Kortei et al. (2018), mushrooms with larger pileus, besides having higher commercial value, will result in higher *BE* and *Pd* values; these researchers found a correlation of d_{pil} with *BE* when cultivating *P. ostreatus* in composted sawdust. The results obtained in this study indicated, however, a different behavior since the highest d_{pil} values were obtained with runs S6 and S9 (Table 2) in contrast to what was already discussed considering the best results for *Pd* (and *BE*, consequently). The adjustment of a quadratic model to the d_{pil} data was statistically significant (p-value < 0.10), however, the R^2 and R_{adj}^2 values were lower (< 0.45) and the Lack of Adjustment was statistically significant (p-value < 0.10), nevertheless, the analysis continued for the purpose of better understanding the effect of the residues over d_{pli}.

According to the Contour Curve obtained (Figure 1c), in order to increase d_{pil} it would be necessary to work with lower *SG* and higher *HT* and *RY*. Inside this region are located the runs S3, S6 and S9 and a narrow band around S2 (C/N = 33 - 39 g/g). This result suggests that, for *P. ostreatus* CCBIt 2339, higher *HT* and *CP* may induce the development of larger pileus, but with lower *BE* and *Pd*, as it can be observed when comparing runs S9 and S5 (Table 2).

Regarding the fact that it is always desirable to reduce the total time of a process to increase its productivity and lower the risks for contamination, t_{mr}, t_{ap} and t_{ch}, were analyzed individually in a similar way as described so far, although, the obtained Contour Curves will not be presented and only the results will be discussed. Values of t_{mr} between 15 and 19 days (Table 2) indicated a shorter mycelial running phase, in comparison to what was obtained by Kumari and Achal (2008) with *P. ostreatus* (20 days) and this response was favored by the same range of compositions that favored the responses *Pd* and *BE*. The substrates S2, S3 and S4 (Table 2) indicated to increase t_{cm} to more than 22 days which is more similar to what was obtained for *P. ostreatus* (22 - 26 days) by Sharma et al. (2013).

It was observed that an increase in *HT* indicated an undesirable increase in t_{ap} values (similar to the analysis of d_{pil}). Shorter t_{ap} values (1 – 5 days) were obtained with S1 and S5 (Table 3) which are around to the 3 days required by *Pleurotus sajor-caju* in onion juice waste (Pereira et al., 2017) but less than what was observed (9 to 17 days) with *P. ostreatus* in weeds (Das and Mukherjee, 2007). According to the results, t_{ch} varied from 30 to 45 days (Table 3) as a consequence of t_{mr} and t_{ap} values.

Ultimately, besides S11, S5 was also chosen for experimental validation, in triplicate, and the obtained responses are presented in Table 3. Considering that some operational difficulties

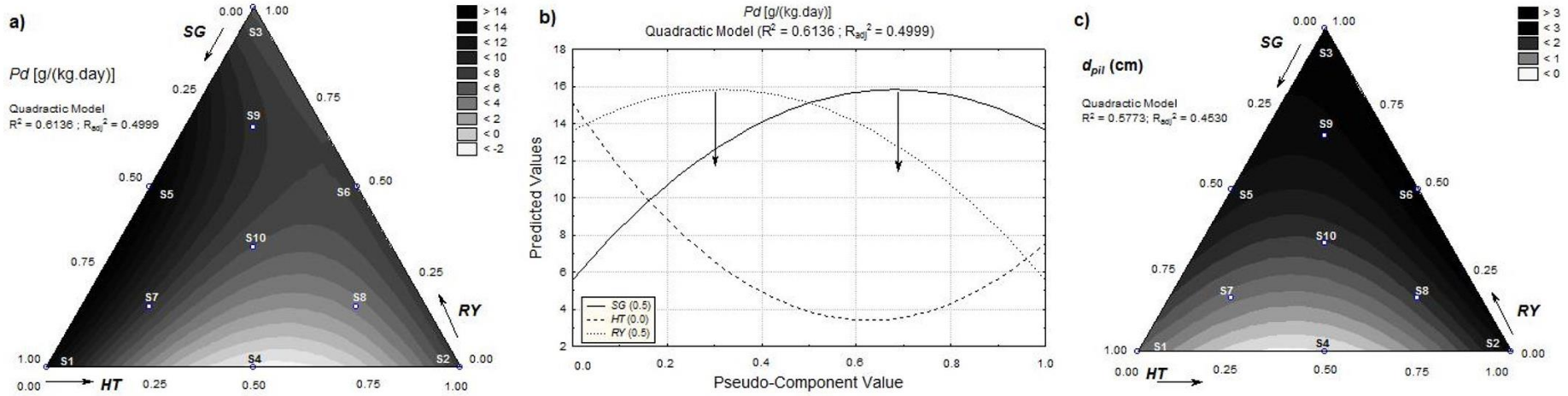

Figure 1. (a) Contour Curve obtained for productivity [*Pd*, g/(kg.day)] considering the coded composition of: brewer's spent grain (*SG*), hot trub (*HT*) and residual brewer's yeast (*RY*) and (b) the relation between the predicted values and the coded levels for a reference blend value of *SG* = *RY* = 0.5 and *HT* = 0.0 and (c) the Contour Curve obtained for pileus diameter (d_{pli}, cm).

Table 3. Biological efficiency (*BE*), productivity (*Pd)*, pileus diameter (d_{pil}) and times for: mycelium running (t_{mr}), appearance of primordia (t_{ap}) and cultivation and harvest (t_{ch}) obtained for the cultivation of *Pleurotus ostreaturs* CCIBt 2339 on substrates (S5 and S11) containing brewer's residues and cocoa pod shells.

Substrate	Responses*					
	***EB* (g/kg)**	***Pd* [g/(kg.day)]**	**d_{pil} (cm)**	**t_{mr} (days)**	**t_{ap} (days)**	**t_{ch} (days)**
S5	437.8 ± 142.5[a]	11.8 ± 9.8[a]	2.1 ± 0.5[a]	27.0 ± 0.0[a]	6.6 ± 1.0[a]	37.0 ± 0.0[a]
S11	1,204.4 ± 207.8[b]	32.6 ± 18.7[b]	3.2 ± 0.5[b]	22.0 ± 0.0[b]	3.5 ± 1.0[b]	37.0 ± 0.0[a]

*Mean values ± standard deviation, from triplicates. Values with different superscript letters, in the same column, are significantly different ($p < 0.05$).

were faced to maintain humidity inside the fruiting room for the first couple of days of cultivation and acknowledging the inherent variability of the experiments, substrate S11 (defined with the statistical analysis) was considered the best condition for *P. ostreatus* CCIBt 2339 cultivation. In comparison to S5, the increase in *SG* and the decrease in *RY* and *CP* resulted in a C/N ratio 6% lower and a *Pd* around 2.8 times higher (Table 3).

Enzymatic screening

The enzymatic screening for the obtained crude multi-enzymatic extracts (CMEs) is presented in Table 4, from which it is possible to identify the biotechnological potential of each CME, especially in relation to the activities of laccase, xylanase, pectinase and amylase. In general, the reduction of *SG* (%, w/w) from 90% (S1) to 58% (S11) associated with the increase of *CP* and *RY* (Table 2), indicated to be positive for the production of laccases and amylases. However, when considering to reduce *SG* even more, from 58% (S11) to 50% (S5) also associated with the increase of *CP* and *RY*, that indicated not to be beneficial for laccases, amylases and pectinases (Table 4). Regarding S9, the only condition with *HT* and the highest *CP*, the lowest laccase,

Table 4. Enzymatic screening of crude multi-enzymatic extracts obtained after the mycelial running of *Pleurotus ostreatus* CCIBt 2339 cultivated on different substrates (S1, S5, S9 and S11) containing brewer's residue and cocoa pod shells.

Substrate	Enzymatic activities (U/g)*						
	Laccase	Xylanase	FPase	CMCase	Pectinase	Amylase	Tannase
S1	2,073.3 ± 0.03^{a}	110.4 ± 0.01^{a}	< 0.5	6.7 ± 0.05^{a}	370.7 ± 0.0^{a}	4.5 ± 0.01^{a}	< 0.5
S5	3,977.7 ± 0.04^{b}	100.8 ± 0.06^{a}	< 0.5	5.3 ± 0.03^{b}	96.8 ± 0.00^{b}	2.0 ± 0.01^{b}	< 0.5
S9	1,086.6 ± 0.01^{c}	1.6 ± 0.00^{b}	< 0.5	5.1 ± 0.01^{b}	2.2 ± 0.03^{c}	3.1 ± 0.02^{c}	< 0.5
S11	7,644.4 ± 0.04^{d}	110.9 ± 0.02^{a}	< 0.5	4.6 ± 0.02^{c}	126.1 ± 0.05^{d}	277.4 ± 0.06^{d}	< 0.5

*Mean values ± standard deviation, from triplicates. Values with different superscript letters, in the same column, are significantly different (p < 0.05).

xylanase and pectinase activities were obtained (Table 4). Between S1, S5 and S11, there were no significant changes in xylanase activities and, for all conditions evaluated, a similar CMCase production was obtained (Table 4).

Laccases, xylanases, FPases and CMCases are enzymes investigated for the degradation of lignocellulosic substrates. It was reported for *P. ostreatus*, for instance, that nitrogen supplementation of soybean hulls could result in an increase in laccase production, in this case, the highest activities (60 - 80 U/g) were reached at a much lower C/N (5.0 g/g) (D´Agostini et al., 2011). In another example, a co-cultivation of *P. ostreatus* MTCC 180 and *Penicillium oxalicum* SAUE-3.510 in sugarcane bagasse and bean husk resulted in a higher yield of xylanase (8,205.31 U/g) (Dwivedi et al., 2011). With cultivation in sesame straw and wheat bran (C/N = 27 g/g), it was possible to obtain a lower activity of CMCase (1.75 U/g) with a substrate with a very similar C/N to S5 (Kurt and Buyukalaca, 2010). Pectinases and amylases are enzymes capable to hydrolyze, for example, mucilages and starches that are naturally found in different vegetable parts. In the spent substrate of *P. sajor-caju* in onion residues (with a much higher C/N of 266.22 g/g) a pectinase activity of around 96 U/g was obtained (Pereira et al., 2017), close to what was obtained with S5 (Table 4). Considering amylases from *Pleurotus*, there are only a few reports in literature, for example, around 9 U/g was reported in a spent substrate of undeclared composition (Nakajima et al., 2018).

All four compositions investigated presented FPase and tannase activities close to the control conditions of the enzymatic methodologies (0.43 < U/g < 0.01), indicating that the extracts obtained did not present expressive activities for these two enzymes. In order to obtain a better quantification, it could be suggested a methodology of greater sensitivity (such as liquid chromatography). However, FPase (22 U/g) and tannase (1 U/g) activities have been reported for *P. ostreatus* when cultivated, respectively, in banana pseudostem supplemented with Tween 80 (Silva et al., 2019) and jatropha biodiesel residues (Luz et al., 2013).

When considering the world production of mushrooms and truffles, which was almost 9 million tons in 2018 (FAOSTAT, 2020), it is possible to understand that the spent substrate produced, accumulated or sub-utilized still has a great biotechnological value that needs to be better explored. For that reason, the enzymatic profiles obtained (Table 4) can indicate the potential for the spent substrates as a source of important enzymes (Nakajima et al., 2018; Pereira et al., 2017).

Conclusions

When working with different residues to compose a substrate for mushroom cultivation, it is important to investigate the best composition since it can modulate different responses related to growth. In this study it was possible, with the help of a statistical tool, to detect the advantages of balancing the compositions of brewer's spent grain and cocoa pod shells and it also permitted to choose the residual brewer's yeast over the hot trub in order to improve, for example, productivity and laccase activity. Thus, it is reinforced that the proper use of agro-industrial residues to produce edible mushrooms is a viable, necessary and a low-impact practice since it is possible to produce a nutritional food and obtain important enzymes from the spent substrate.

CONFLICT OF INTEREST

The authors have not declared any conflict of interests.

ACKNOWLEDGEMENTS

The authors are grateful for the financial support of the Fundação de Amparo à Pesquisa do Estado da Bahia (FAPESB, Brazil) and the Coordenação de Aperfeiçoamento de Pessoal de Nível Superior (CAPES, Brazil) and for the experimental support from the Centro de Inovação do Cacau (CIC, Ilhéus, BA, Brazil).

REFERENCES

Adjin-Tetteha M, Asiedua N, Dodoo-Arhin D, Karam A, Amaniampong

PN (2018). Thermochemical conversion and characterization of cocoa pod husks a potential agricultural waste from Ghana. Industrial Crops and Products 119:304-312.
Antwi E, Engler N, Nelles M, Shüch A (2019). Anaerobic digestion and the effect of hydrothermal pretreatment on the biogas yield of cocoa pods residues. Waste Management 88:131-140.
Castellani A (1967). Maintenance and cultivation of common pathogenic fungi of man in sterile distilled water. Further Researches. The Journal of Tropical Medicine and Hygiene 70:181-184.
D´Agostini EC, Mantovanti CE, Valle JS, Meirelles LD, Colauto NB, Linde G (2011). Low carbon/nitrogen ratio increases laccase production from basidiomycetes in solid substrate cultivation. Scientia Agricola 68(3):295-300.
Das N, Mukherjee M (2007). Cultivation of *Pleurotus ostreatus* on weed plants. Bioressource Technology 98(14):2723-2726.
Dwivedi P, Vivekanand V, Pareek N, Sharma A, Singh RP (2011). Co-cultivation of mutant *Penicillium oxalicum* SAUE-3.510 and *Pleurotus ostreatus* for simultaneous biosynthesis of xylanase and laccase under solid-state fermentation. New Biotechnology 28(6):616-626.
Ergun SO, Urek RO (2017). Production of ligninolytic enzymes by solid state fermentation using *Pleurotus ostreatus*. Annals of Agrarian Science 15(2):273-277.
FAOSTAT (2020). Food and Agriculture Data - Food and Agriculture Organization of the United Nation (FAO). Available at: http://www.fao.org/faostat/en/#data - last consult on September 3rd, 2020.
Fonseca TRB, Alecrim MM, Cruz Filho RFC, Teixeira MFS (2015). Cultivation and nutritional studies of an edible mushroom from North Brazil. African Journal of Microbiology Research 9(30):1814-1822.
Ghose TK, Bisaria VS (1987). Measurement of hemicellulase activities. Part 1: 472. Xylanases. Pure and Applied Chemistry 591:739-52.
Hassan SS, Ravindrana R, Jaiswal S, Tiwari BK, William GA, Jaiswal AK (2020). An evaluation of sonication pretreatment for enhancing saccharification of brewers' spent grain. Waste Management 105:240-247.
Instituto Adolfo Luts (IAL) (2008). *Métodos físico químicos para análise de alimentos*. 4th Ed. Instituto Adolfo Lutz, São Paulo.
Kortei KN, Odamtten TG, Obodai M, Kwagyan-Wiafe M, Mensah NLD (2018). Correlations of cap diameter (pileus width), stipe length and biological efficiency of *Pleurotus ostreatus* (Ex.Fr.) Kummer cultivated on gamma-irradiated and steam-sterilized composted sawdust as an index of quality for pricing. Agriculture and Food Security 7:35.
Kumari D, Achal V (2008). Effect of different substrates on the production and nonenzymatic antioxidant activity of *Pleurotus ostreatus*. Life Science Journal 5:73-76.
Kurt S, Buyukalaca S (2010). Yield performances and changes in enzyme activities of *Pleurotus* spp. (*P. ostreatus* and *P. sajor-caju*) cultivated on different agricultural wastes. Bioresource Technology 101(9):3164-3169.
Lu L, Zeng G, Fan C, Ren X, Wang C, Zhao Q (2013). Characterization of a laccase like multicopper oxidase from newly isolated *Streptomyces* sp. C1 in agricultural waste compost and enzymatic decolorization of azo dyes. Biochemical Engineering Journal 72:70-76.
Luz JMR, Paes SA, Torres DP, Nunes MD, Silva JS, Mantovani HC, Kasuya MCM (2013). Production of edible mushroom and degradation of antinutritional factors in jatropha biodiesel residues. LWT - Food Science Technology 50(2):575-580.
Marino RH, Abreu LD (2009). Cultivation of mushroom Shiitake in coconut wastes supplemented with bran or/and rice bran. Revista Brasileira de Ciências Agrárias 4(1):11-16.
Mattioli S, Castellini C, Mancini S, Roscini V, Mancinelli AC, Cotozzolo E, Pauselli M, Bosco AD (2020). Effect of trub and/or linseed dietary supplementation on in vivo oxidative status and some quality traits of rabbit meat. Meat Science 163:108061.
Nakajima VM, Soares FEF, Queiroz JH (2018). Screening and decolorizing potential of enzymes from spent mushroom composts of six different mushrooms. Biocatalysis and Agricultural Biotechnology 13:58-61.
Oliveira MA, Donega MA, Peralta RM, Souza CGM (2007). Production of spawn for edible mushroom *Pleurotus pulmonarius* (Fr.) Quélet - CCB19 using agricultural wastes. Ciência e Tecnologia de Alimentos 27(1):84-87.
Pereira GS, Cipriani M, Wisbeck E, Souza O, Strapazzon JO, Gern RMM (2017). Onion juice waste for production of *Pleurotus sajor-caju* and pectinases. Food and Bioproducts Processing 106:11-18.
Puligundla P, Moka C, Park S (2020). Advances in the valorization of spent brewer's yeast. Innovative Food Science and Emerging Technologies 62:102350.
Rojas-Chamorro JA, Romero I, López-Linares JC, Castro E (2020). Brewer's spent grain as a source of renewable fuel through optimized dilute acid pretreatment. Renewable Energy 148:81-90.
Sharma S, Yadav RKP, Pokhrel CP (2013). Growth and yield of oyster mushroom (*Pleurotus ostreatus*) on different substrates. Journal of New Biological Reports 2(1):03-08.
Sharma S, Bhat KT, Dawara KR (2000). A spectrophometric method for assay of tannase using rhodanine. Analytical Biochemistry 279:85-89.
Shet VB, Nisha sanil, Bhat M, Naik M, Mascarenhas LN, Goveas LC, Rao CV, Ujwal P, Sandesh K, Aparna A (2018). Acid hydrolysis optimization of cocoa pod shell using response surface methodology approach toward ethanol production. Agriculture and Natural Resources 52(6):581-587.
Silva IF, Luz JMR, Oliveira SF, Queiroz JH, Kasuya MCM (2019). High-yield cellulase and LiP production after SSF of agricultural wastes by *Pleurotus ostreatus* using different surfactants. Biocatalysis and Agricultural Biotechnology 22:101428.
Shibata C, Demiate I (2003). Cultivation and chemical analysis of the sun mushroom (*Agaricus blazei* Murril). Publication UEPG 9(2):21-32.
Stamets P (2005). Mycellium running – How mushrooms can help save the world. Ten Speed Press, New York.
STATISTA (2020). Leading 10 countries in worldwide beer production in 2018. Available at: https://www.statista.com/statistics/270269/leading-10-countries-in-worldwide-beer-production/ – last consult on September 3rd, 2020.
Umsza-Guez MA, Díaz AB, Ory I, Blandino A, Gomes E, Caro I (2011). Xylanase production by *Aspergillus awamori* under solid state fermentation conditions on tomato pomace. Brazilian Journal of Microbiology 42:1585-1597.
Vasconcelos NM, Pinto GAS, Aragão FAS (2013). *Boletim de Pesquisa n. 88, Determinação de Açúcares Redutores pelo Ácido 3,5-Dinitrosalicílico: Histórico do Desenvolvimento do Método e Estabelecimento de um Protocolo para o Laboratório de Bioprocessos*. EMBRAPA Agroindústria Tropical, Fortaleza.

Vol. 20(3), pp.122-133, March, 2021
DOI: 10.5897/AJB2020.17247
Article Number: 9A8ADFD66364
ISSN: 1684-5315

http://www.academicjournals.org/AJB

ACADEMIC JOURNALS
expand your knowledge

African Journal of Biotechnology

Full Length Research Paper

Adsorption of copper (II) ions onto raw *Globimetula oreophila* (Afomo ori koko) leaves

Chijioke John Ajaelu[1*] and Esther Oremeiyi Faboro[1]

Department of Chemistry and Industrial Chemistry, Bowen University, Iwo, Osun State, Nigeria.

Received 17 September, 2020; Accepted 5 January, 2021

This study examined the adsorption of copper onto raw *Globimetula oreophila* leaves. The adsorbent surface nature was examined using scanning electron microscopy and Fourier transform infrared spectroscopy. Adsorption parameters such as the $-\log_{10}[H^+]$, point of zero charge, initial metal concentration, mass of biomass and contact time were determined. Copper adsorption decreased gradually with pH. The point of zero charge (PZC) obtained was 4.5. The percentage adsorption capacity increased from 97.6 to 99.3% as the initial amount of copper rose from 20 to 100 mg/L. Temkin isotherm gave the best fit (R^2=0.99) in describing the adsorption equilibrium process. Contact time effect resulted in an equilibrium attained in 15 min due to the initial rapid increase in adsorption. Kinetic data were excellently fitted to the pseudo-second order model. Thermodynamic studies affirmed a spontaneous and endothermic adsorption process. The activation energy and the energy of adsorption obtained affirmed that the adsorption process was chemisorption. *G. oreophila* is a recommendable adsorbent for the remediation of copper contaminated soil.

Key words: *Globimetula oreophila*, kinetics, adsorption, isotherm, copper.

INTRODUCTION

Toxic metals availability in the environment are major problem to the world because of its adverse effect on human race. These metals even in trace amount are very harmful to man and his environment. They are persistent in the environment and cannot be degenerated or destroyed. They are found to aggregate in the soil, sediment, seawater and freshwater (Chowdhury and Saha, 2012). The effluents containing heavy metals are discharged into water bodies. Culpable industries are paints and pigments, refineries, metal cleaning and plating baths, fertilizer, paper board mills, wood preservatives, printed circuit board production, pulp, wood pulp production (Chowdhury and Saha, 2012; Zhu et al., 2009, Alao et al., 2014).

Copper is one of the most harmful metals to man and animals if it exceeds the permissible levels. The copper levels in drinking water based on the study from Europe, Canada and USA range from ≤0.005 to >30 mg/L, with the primary source most often being the corrosion of interior copper plumbing (US EPA, 1991; Health Canada, 1992; IPCS, 1998; US NRC, 2000; WHO, 2004). The effluents from industries mostly have high amount of copper (II) ion (Tong et al., 2011). Human ingestion of excess copper ions may lead to possible necrotic

*Corresponding author. E-mail: ajaelujohn2005@yahoo.co.uk, faboro@yahoo.com.

changes in the liver and kidney, gastrointestinal irritation, central nervous problems, hepatic and renal damage, mucosal irritation, severe liver and brain damages, widespread capillary damages and depression (Ajaelu et al., 2017a; Ajmal et al., 1998; Larous et al., 2005).

Several methods available for reducing or totally removing the heavy metal from industrial wastewater include chemical precipitation, evaporation, ion exchange, reverse osmosis, filtration, solvent extraction, oxidation and electro deposition (Tong et al., 2011; Wang and Qin, 2005). The constraint associated with these procedures include the difficulty in removing low amount of heavy metals, inability to apply this method to considerable range of pollutants, it is not cost effective and mostly used for ex-situ amelioration (Ahmada et al., 2014). The use of activated carbon for adsorption is seen as effective but it is quite costly.

Globimetula oreophila is a member of the Loranthaceae family of parasitic mistletoes. Their leaves are greenish. 1000 species and about 75 genera are present in the Loranthaceae *family. G. oreophila* are found in the South West, South- South and South East of Nigeria. They are also found in the North West of Cameroon. All mistletoes species are members of the Loranthaceae family except those of North America and Europe*.* More than 60 species of the family have been located in West Africa. Some of the trees on which *G. oreophila* are found include cocoa tree, rubber tree and orange tree among others. It is acclaimed by the traditional health practitioners in Nigeria that the extracts of *G. oreophila* are employed in the prevention, treatment and management of cardiovascular related diseases and ailments (Faboro et al., 2018).

This study investigated the viability of *G. oreophila* for the adsorption of copper (II) ions from simulated waste water. Parameters studied included the effects of biomass, pH, point of zero charge and initial metal concentrations. Adsorption kinetics and effect of temperature were also studied.

MATERIALS AND METHODS

G. oreophila leaves were harvested from Cocoa tree in Ondo State, Nigeria. The chemicals used include $CuSO_4.5H_2O$, HCl and NaOH. All these chemicals are of analytical grade.

Biomass preparation

The *G. oreophila* leaves were washed with distilled water and air dried after which they were oven-dried at 105°C overnight. Pulverization of the dried leaves was carried out followed by the screening through a 1 mm sieve to obtain the geometric size and then stored in an air tight plastic bag.

Adsorption studies

Biosorption procedures were carried out by varying the amounts of solution pH, initial Cu (II) ions concentration (having a pH of 4.57), mass of adsorbent, contact time and temperature under batch experiments. Adjustment of the solution pH was done by adding either 0.1 M NaOH or 0.1 M HCl solutions before adsorption experiment. The experiments took place on a Stuart Orbital Shaker at 250 rpm. The amount of Cu (II) ions was obtained using Atomic Absorption spectrophotometer (PG 990, PG instruments, Britain). The studies were performed in duplicate and the average value was used for later calculation.

The amount of *G. oreophila* adsorbed was given by:

$$q = \frac{(C_o - C_e)}{W} xV \quad \text{(i)}$$

$$\% \text{ adsorption capacity } = \frac{(C_o - C_e)}{C_o} x100 \quad \text{(ii)}$$

Where q(mg/g) is the adsorption capacity, C_o (mg/L) and C_e (mg/L) are the initial Cu^{2+} ion concentration and equilibrium Cu^{2+} ion concentration respectively, V(L) is the volume while W (g) is the mass of the adsorbent.

RESULTS AND DISCUSSION

SEM and FTIR analysis

The surface structure was characterized by SEM as presented in Figure 1. The surface has irregular, flat sheets containing some pores. The irregular sheets are in layers. There may be the possibility of the adsorbent having a microporous and a mesoporous surface. Functional groups are possible adsorption sites for dyes. FTIR analyses of raw *G. oreophila* without and with copper as presented in Figure 2a and b reflect the following functional groups: Vibrational frequency appeared between 3514.9 and 3941.7 cm^{-1} attributed to the O-H stretching which shifted from 3520.5 to 3893.2 cm^{-1} for adsorbent with copper. The band at 3384.4-3514.9 cm^{-1} attributed to the N-H stretch shifted to 3230.7-3503.7 cm^{-1} in the *G. oreophila* with copper. The bands at 1636.3 - 1653.1 cm^{-1} corresponding to C=O of amide were shifted to 1638.2 - 1684.8 cm^{-1} for adsorbent with copper. The band at 1375.4 cm^{-1} for adsorbent without copper was shifted to 1319.5-1362.3 cm^{-1} for adsorbent with copper and is assigned to C-H rock of alkane. The band observed at 1164.8 - 1217.0 cm^{-1} for adsorbent without copper are attributed to -C-O stretch of alcohol was shifted to 1036.3 - 1217.0 cm^{-1} for adsorbent with copper. The band observed at 1164.8 - 1217.0 cm^{-1} for adsorbent without copper are attributed to -CN stretch aliphatic amine was shifted to 1036.3 - 1217.0 cm^{-1} for adsorbent with copper. These results show that the major functional groups responsible for the adsorption process are amide, amine and alcohol.

Effect of pH

The pH of solution has played a major role in the

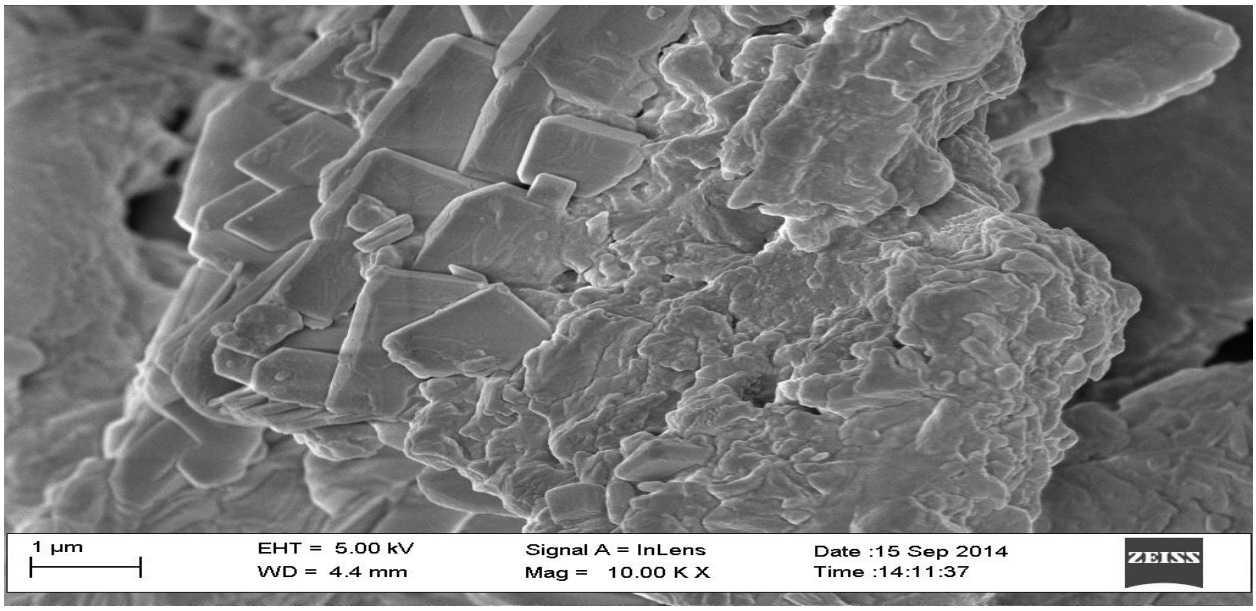

Figure 1. SEM of raw *G. oreophila.*

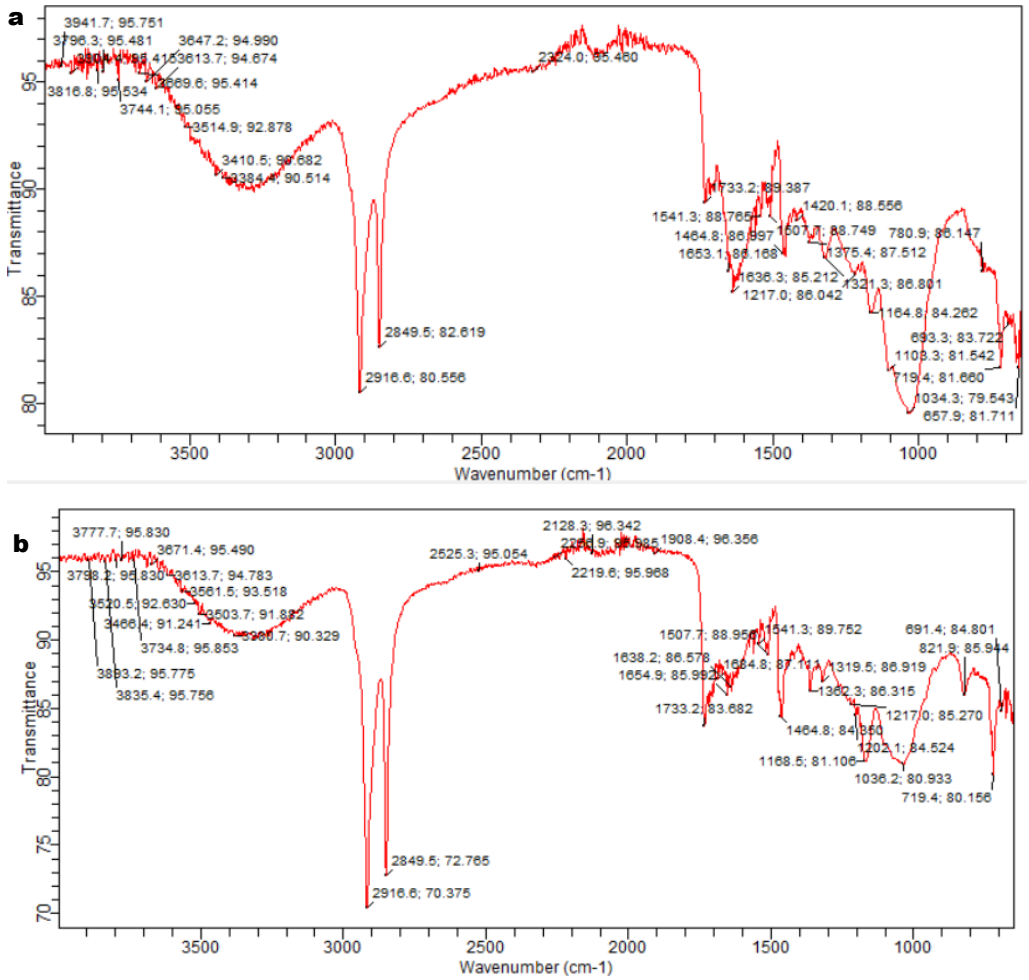

Figure 2. FTIR of *G. oreophila* (a) before adsorption; (b) after adsorption of copper (II) ions.

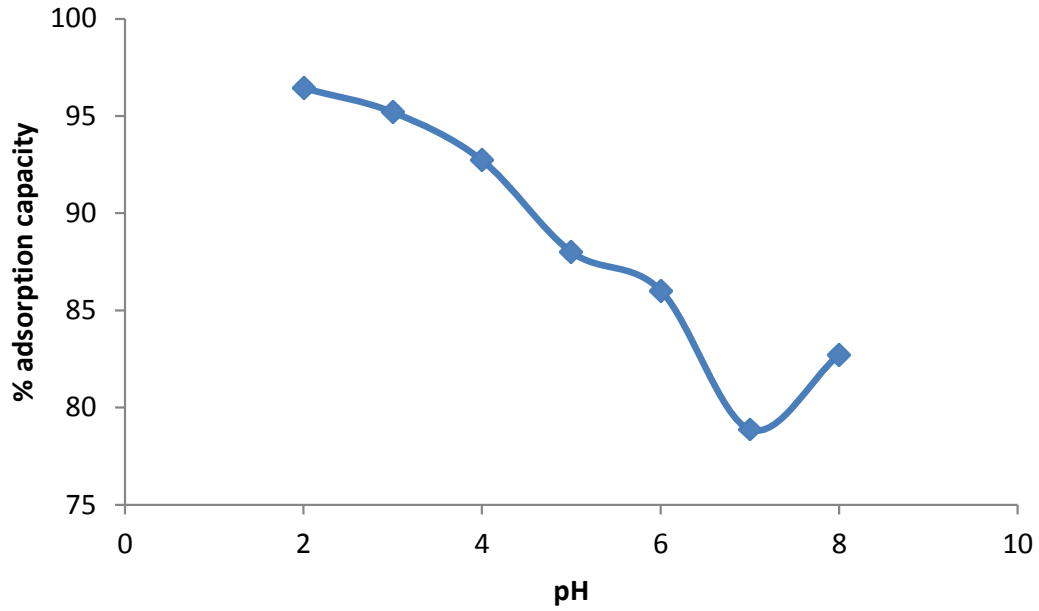

Figure 3. pH effect on the sorption of copper on *G. oreophila*.

adsorption of heavy metals from aqueous solution and consequently waste water. The effect of pH was considered in the range 2.0 to 8.0 as seen in Figure 3. The pH at which the net surface charge on an adsorbent is zero is referred to as the point of zero charge, PZC. When the pH value is lower than PZC the number of negatively charged sites on the adsorbent reduces which results in the increase in the number of positively charged sites which enhances the adsorption of anions. At pH values greater than PZC, there is increase in the number of negatively charged sites on the surface of the adsorbent such that the extent of adsorption of cations increases because of ionic attraction between the negatively charged surface and the cationic adsorbate. The result obtained is quite surprising. Percentage adsorption increases with decrease in pH. The PZC obtained for *Globimetula oroephila* is 4.5 as shown in Figure 4. Below that value, the surface of the adsorbent is expected to be positively charged and the adsorbate is also positively charged. Possible explanation is that there may be some negatively charged functional groups responsible for the attraction and increase.

Initial copper concentration

Initial metal concentration has significant effect on the adsorption of metals by adsorbents. Figure 5 shows that percentage adsorption capacity increased from 97.6 to 99.3% as the initial metal concentration increased from 20 to 100 mg/L. This can result from the fact that at higher initial copper concentrations more vacant sites are available for adsorption. The variant concentrations enable the essential driving force to overwhelm the mass transfer of copper (II) ions between the solid and aqueous phases.

Effect of mass of biomass

Adsorbent mass is known to affect the capacity of adsorption of various adsorbents. Figure 6 reports the adsorptive removal of Cu(II) ions by *G. oreophila*. Adsorption capacity of *G. oreophila* reduces with a rise in the mass of biomass. The reduction in the amount of copper adsorbed at the surface of *G. oreophila* with increase in mass of biomass can be ascribed to the concentration gradient or split in the flux between the amount of copper in the solution and that on the surface. Therefore, the amount of copper adsorbed onto unit mass of adsorbent (*G. oreophila*) reduces as the adsorbent weight rises, thus leading to a reduction in the amount of Cu(II) ions adsorbed (q_e) as the weight of adsorbent rises. Similar findings had been described by Ajaelu et al. (2017a) and Zafar et al. (2006).

Adsorption isotherms

Equilibrium adsorption isotherms are vital in designing adsorption process for they strongly imply metal ions distribution between the phases that are liquid and the adsorbent at equilibrium with respect to the metal concentration. Each time an adsorbent contacts a solution of metal ion, the surface of the adsorbent experiences a sudden rise in the concentration of metal ions until a

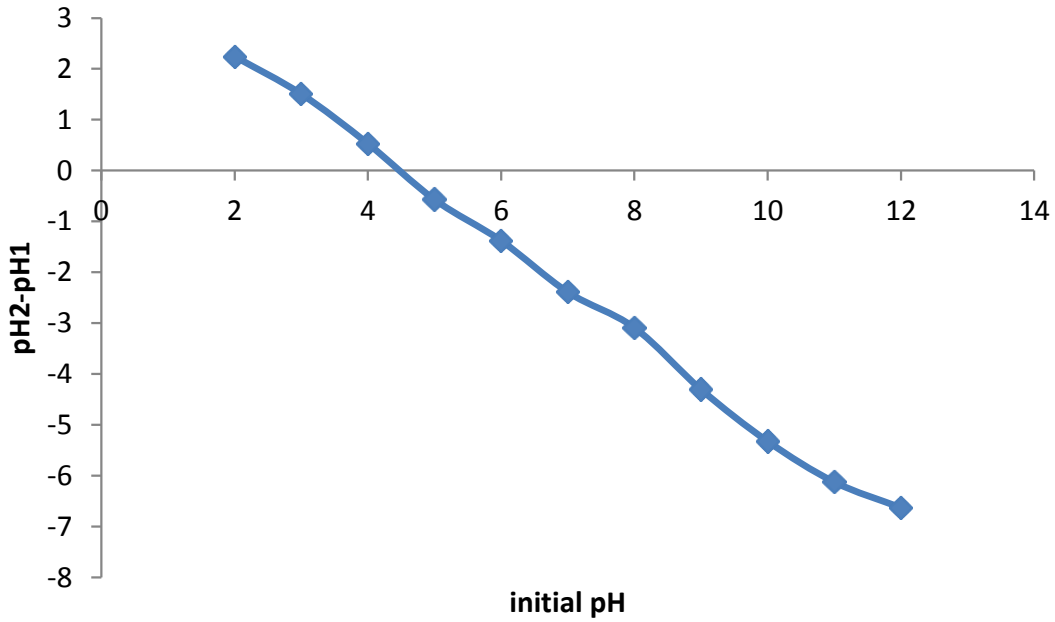

Figure 4. Point of zero charge effect on copper (II) ions biosorption onto *Globimetula oreophila.*

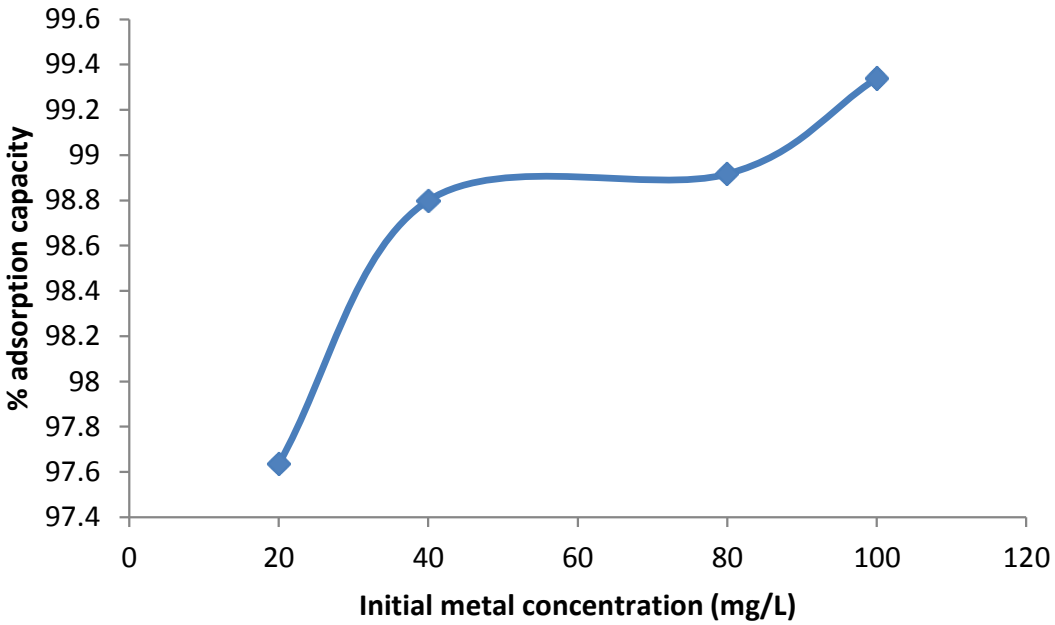

Figure 5. Initial metal concentration effect on the adsorption of copper on *Globimetula oreophila.*

dynamic equilibrium is attained. Four biosorption models specifically, Langmuir, Freundlich, Temkin and Dubini-Radushkevich were employed to describe the adsorption of copper on *G. oreophila*. The Langmuir model surmises that adsorption sites are equivalent and adsorption at each site is not dependent on adsorption or desorption at adjacent sites. The linear expression of the Langmuir equation is as follows:

$$\frac{C_e}{q_e} = \frac{1}{Q_o b} + \frac{1}{Q_o} C_e \quad (3)$$

Where C_e and q_e are the amount of solute in the solution at equilibrium ((mg/L) and the amount of solute adsorbed per unit mass of adsorbent (mg/g), respectively. Q_o (mg/g) refers to the highest level of monolayer uptake

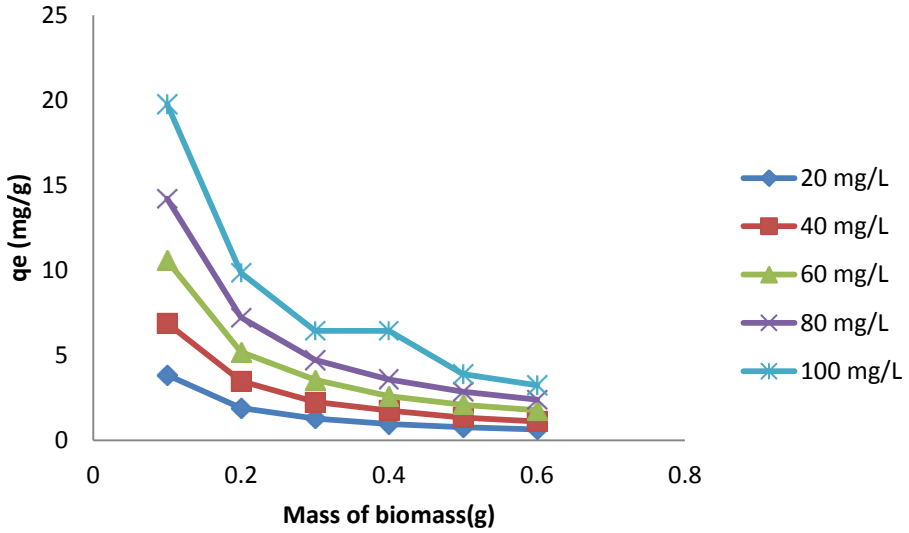

Figure 6. Mass of biomass effect on the adsorption of copper by *Globimetula oreophila.*

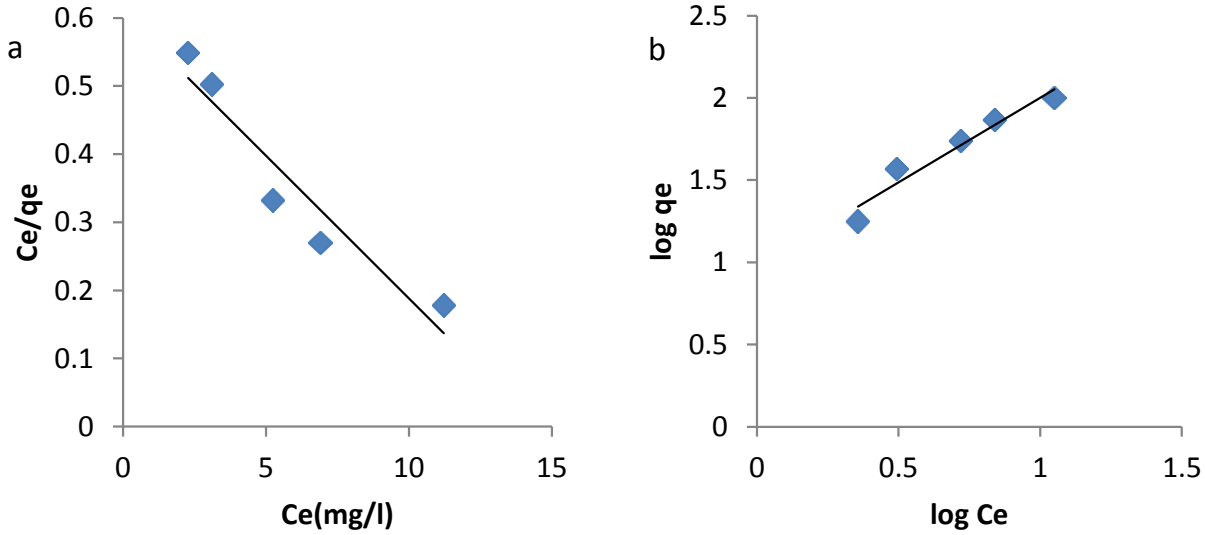

Figure 7. (a) Langmuir and (b) Freundlich isotherms for the adsorption of copper onto *G. oreophila.*

capacity and b (L/mg) is a constant associated with the free energy of adsorption. Figure 7a presents the graph of C_e/q_e and the amount at equilibrium (C_e). The slope and intercept from the plot were used to calculate the values of Q_o and b as presented in Table 1. A dimensionless equilibrium factor, R_L that describes the favourability of adsorption was obtained from the expression (Weber and Chakkravort, 1974).

$$R_L = \frac{1}{(1+C_o)} \quad (4)$$

R_L value calculated as reported in Table 1 shows that the adsorption of copper by *G. oreophila* was favourable since its value is between 0 and 1. The Freundlich expression assumes a heterogeneous surface adsorption. The linear expression for the Freundlich isotherm is:

$$\log q_e = \log K_x + \frac{1}{v}\log C_e \quad (5)$$

Where K_x is a constant which is a measure of the relative uptake capacity of the adsorbent and v' is a constant which is a measure of adsorption intensity as well as the heterogeneous nature of the surface of the adsorbent. Values of K_x and v, were obtained from the plot of log q_e

Table 1. Freundlich, Langmuir, Temkin and Dubinin–Radushkevich Isotherms for the adsorption of copper on *G. oreophila.*

Langmuir	Freundlich	Temkin	D-R
Q_o = 23.9 mg/g	K_x = 9.40	A = 0.65 mg/g	q_x = 1.05 mg/g
b = 0.069 L/mg	v = 1.00	B = 48.2	β = 2.8 x 10^{-3}
R^2 = 0.91	R^2 = 0.94	R^2 = 0.99	E = 20.4 kJ/mol
R_L = 0.127			R^2 = 0.95

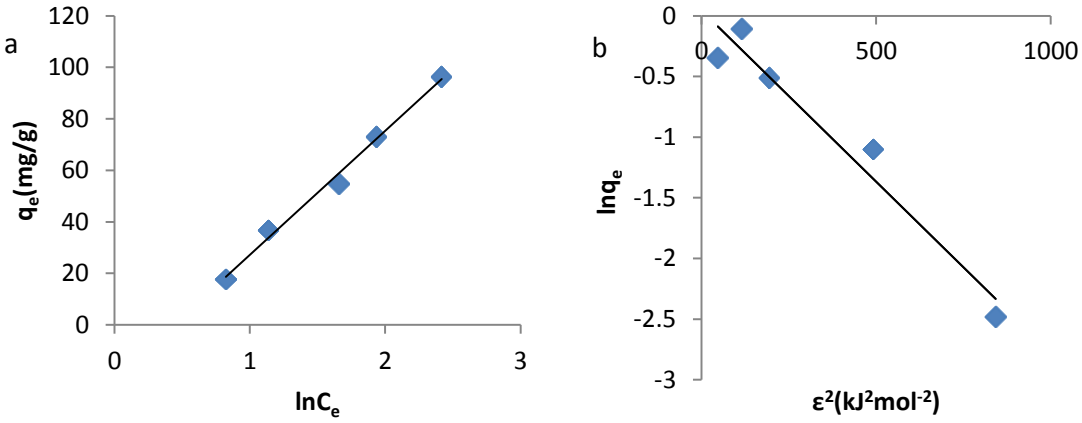

Figure 8. (a) Temkin and (b) Dubinin Rudishkevich isotherms for the adsorption of copper onto *Globimetula oreophila.*

and log C_e as presented in Figure 7b.

The Temkin isotherm (Temkin, 1941) considered the interaction between the adsorbate and the adsorbent. This isotherm assumes a reduction in the heat of biosorption of molecules in the layer. Temkin expression is given as:

$$q_e = B\ln A + B\ln C_e$$

Where $B = \frac{RT}{b}$

The temperature and the gas constant are represented by T(K) and R ($Jmol^{-1}K^{-1}$) respectively. The constant b is associated with the heat of adsorption, A ($Lmol^{-1}$) is the binding constant at equilibrium which is associated with the maximum binding energy (Tong et al., 2011). The plot of q_e versus lnC_e (Figure 8a) helps in the calculation of constants A and B as reported in Table 1.

The Dubinin–Radushkevich (D–R) expression is given by:

$$\ln q_e = \ln q_x - \beta\left[RT\ln\left(1+\frac{1}{C_e}\right)\right]^2 \quad (8)$$

where q_e is the equilibrium amount of copper biosorbed, β is a constant corresponding to the adsorption energy, q_x is the capacity at maximum adsorption, ε is the Polanyi potential, that is equal to:

$$\varepsilon = RT\ln\left(1+\frac{1}{C_e}\right) \quad (9)$$

(6)

Equation 8 can be re-written as:

(7)

$$\ln q_e = \ln q - \beta\varepsilon^2 \quad (10)$$

Table 1 reports the value of R^2 for the plot of q_e against ε^2. The *q* and β values were obtained from the gradient and intercept of the plots (Figure 8b).

The mean free energy of biosorption, E, was calculated from the equation:

$$E = 1/\sqrt{2\beta} \quad (11)$$

The magnitude of *E* explains the ion-exchange, physical or chemical sorption of the adsorption process. As reported by Atkins and Paula (2006), physisorption, can be caused by weak van der Waal interactions between the adsorbent and the adsorbate. The energy of physisorption is in the region of less than 20 kJ/mol.

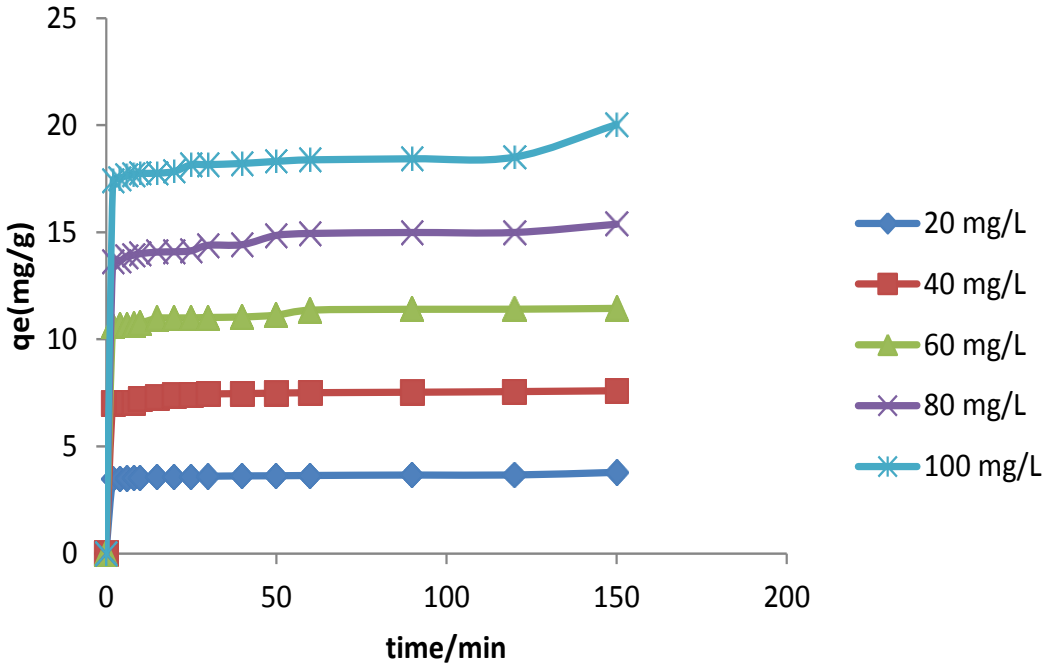

Figure 9. Effect of contact time on the adsorption of copper onto *G. oreophila.*

Atkins added that there is covalent bond between the adsorbate and the adsorbent in chemisorption in which the substrate (adsorbent) is limited to monolayer coverage. The value of E, the mean free energy of biosorption, determined from this study as reported in Table 1 was higher than 20 kJ/mol, thus chemisorption process predominates. Out of the four adsorption isotherms, Temkin isotherm gave the best fit.

Copper adsorption kinetics

Contact time effect

Figure 9 reports the contact time effect on the sorption of copper by *G. oreophila*. Adsorption increases rapidly initially and reached equilibrium in 15 min of mixing of *G. oreophila* with the copper solution. This occurred due to the numerous available active sites on the adsorbent surface and the electrostatic interaction between the positively charged copper (II) ions and the negatively charged surface of *G. oreophila*. As copper (II) ions occupy the sites, electrostatic repulsion gradually increases between the copper (II) ions present in the site and the copper (II) ions present in the solution. This consequently reduces the adsorption of copper (II) ions and thus equilibrium is established.

Kinetic effect on the process of adsorption is vital since it explains the rate of adsorption of the adsorbate which then regulates the contact time of the *G. oreophila* at the solid–solution interface. The kinetics of copper biosorption by *G. oreophila* was analyzed using the Pseudo- first and pseudo-second order models. The Langergren pseudo-first order expression is given below:

$$\log(q_e - q_t) = \log q_e - \frac{k_1}{2.303} t \quad (12)$$

Where q_e and q_t refer to the equilibrium and time t biosorption capacities respectively, of *Globimetula oreophila*; k_1 is the pseudo- first order biosorption rate constant. The plots of log (q_e-q_t) versus t (min) for different copper concentrations give straight lines (Figure 10a). From the plots, k_1 and q_e are obtained from the gradient and intercept respectively as presented in Table 2.

The linear expression of the pseudo-second order kinetic isotherm is given as:

$$\frac{t}{q_t} = \frac{1}{k_2 q_e^{\,2}} + \frac{1}{q_t} t \quad (13)$$

The graph of t/q_t against t is presented in Figure 10b while the parameters of these kinetic models were reported in Table 2. The pseudo-second-order isotherm is more suitable for describing copper adsorption unto *G. oreophila* than the pseudo-first-order isotherm, since it has higher R^2 values (R^2 = 1) and its calculated and experimental values are equivalent. In addition, the authenticity of the kinetic models can be verified by using the normalized standard deviation given by:

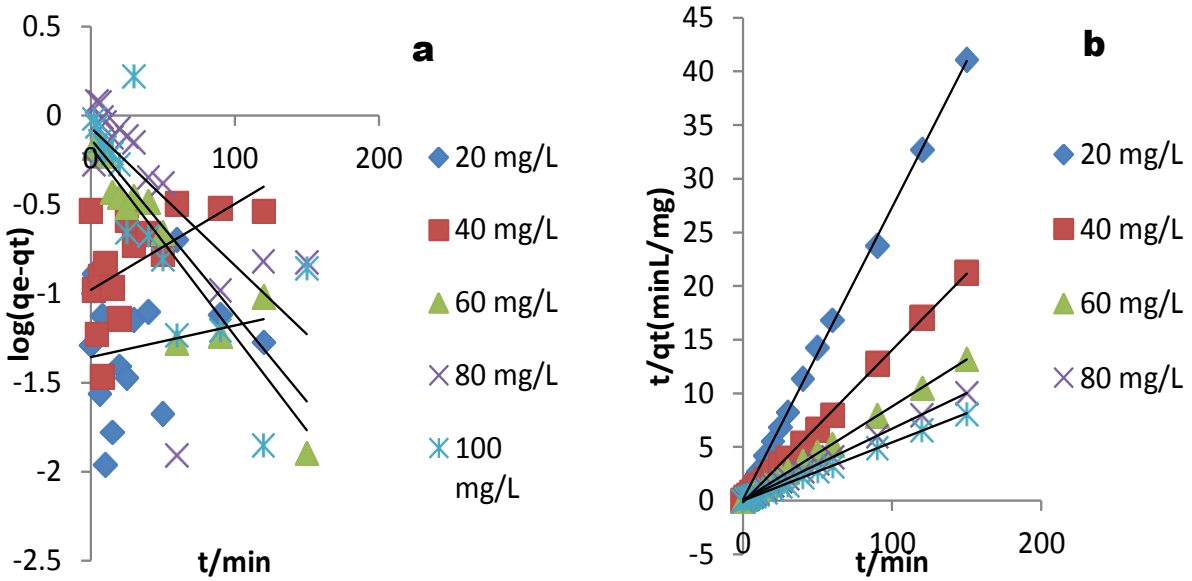

Figure 10. Kinetic plot showing a. Pseudo- first and b. pseudo- second order for copper adsorption onto G. *oreophila.*

Table 2. Pseudo-first and pseudo-second order isotherms for the biosorption of copper on *G. oreophila.*

	Pseudo-first order				Pseudo second order			
Conc (mg/L)	$q_{e(exp)}$ (mg/g)	$q_{e(calc)}$ (mg/g)	k_1/min	Δq	$q_{e\ (calc)}$	k_2 ($gmg^{-1}min$)	Δq	R^2
20	3.59	3.88	0.0018	7.49	3.67	0.704	0.583	1
40	7.34	2.66	0.0048	121	7.04	0.129	1.058	1
60	11.4	1.19	0.1775	262	11.4	0.149	0.178	1
80	14.8	1.07	0.0686	355	15.1	0.072	0.384	1
100	18.4	1.14	0.133	445	18.5	0.249	0.163	1

$$\Delta q = \sqrt{\frac{\sum\left[\left(q_{\exp} - q_{cal}\right)/q_{\exp}\right]^2}{p-1}} x100 \quad (14)$$

Where q_{exp} is the amount of copper (II) ions obtained by experiment and q_{cal} values are the amount of copper (II) ions obtained by calculation, and p is the number of determinations. The low value of Δq corroborates the study that the pseudo-second order kinetic isotherm is better explaining the adsorption kinetics of copper onto *G. oreophila*. Previous study on the adsorbent, *Tectona grandis,* reported similar result (Ajaelu et al., 2017b).

Thermodynamic effect

The temperature effects were investigated at 303, 308, 313 and 318 K. Figure 11 shows that there was a slight reduction in the adsorption capacity as the temperature decreases. This means that the adsorption process was chemisorptions, corroborating the earlier mentioned mean free energy of biosorption obtained from Dubinin-Radushkevich model. The thermodynamic parameters determined were calculated as follows:

$$\Delta G = -RT\ln K \quad (15)$$

$$\ln K = -\frac{\Delta G}{RT} = \frac{\Delta S}{R} - \frac{\Delta H}{RT} \quad (16)$$

The entropy change ΔS as well as the enthalpy change ΔH was calculated from the plot of lnK against 1/T as presented in Figure 12. The K_L values were calculated from the expression $K = q_e/C_e$ at different amounts of Cu (II) ions from 20 to 100 mg/L, and the data are reported in Table 3. The adsorption of copper on *G. oreophila* is spontaneous (ΔG is negative) and endothermic (Δ*H* is positive). Moreover, there is a rise in entropy (ΔS is positive) at the adsorbent-adsorbate interface and this positive value means that the adsorbate species displace the adsorbed solvent molecules to gain more translational entropy than was lost by the adsorbate, thus

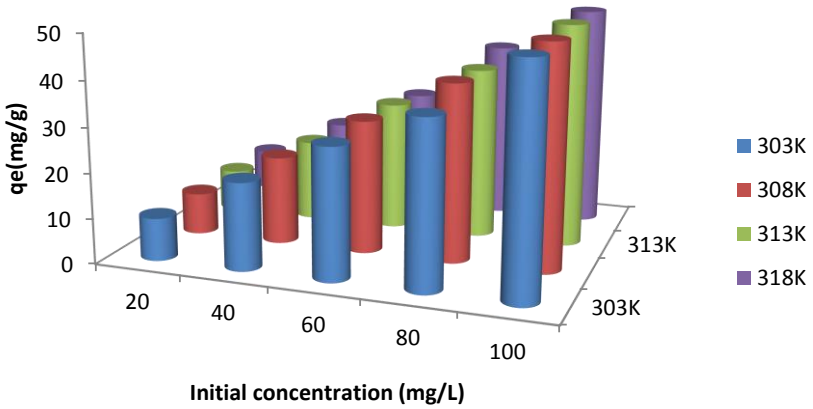

Figure 11. Effect of temperature and initial concentrations on the adsorption of copper by *G. oreophila.*

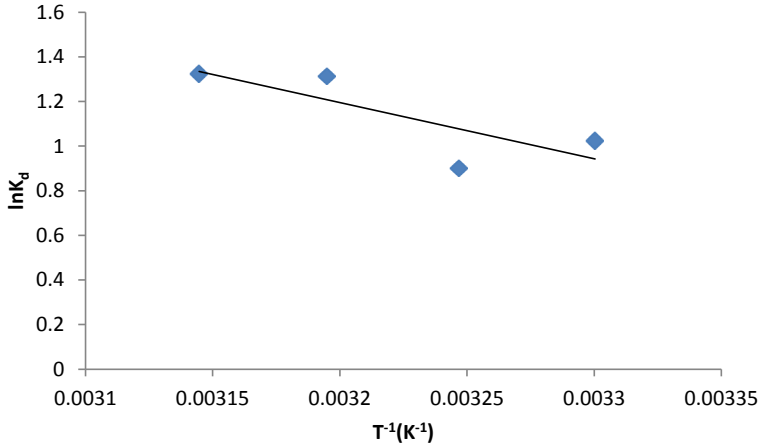

Figure 12. van't Hoff plot for the adsorption of copper by *G. oreophila.*

allowing randomness in the system (Baccar et al., 2013).

The adsorption activation energy was determined using the Arrhenius equation for it denotes the minimum energy required for the adsorption reaction to proceed. The equation is given by:

$$\ln k = \ln A - \frac{E_a}{RT} \quad (17)$$

The value of E_a (168.3 kJmol^{-1}) falls in the energy range of 40 to 800 kJ/mol, which means that chemisorption is the process of adsorption.

Ionic strength effect

Ionic strength has significant effect on the adsorption process. Figure 13 presents the influence of ionic strength on the adsorption capacity of copper unto *G. oreophila*. As the ionic strength increases from 0.02 to 0.08 moldm^{-3}, the capacity of adsorption increased from 231 to 1620 mg/g. This shows that adsorption increases with increase in ionic strength. This result is contrary to what was obtained by some researchers. These may be due to accessibility modification of the functional group sites that binds metals on the *G. oreophila* surface as well as the modification in the activity of the aqueous metal cations as a function of ionic strength (Borrok and Fein, 2005).

Conclusion

This study investigated the adsorption efficiency of raw *G. oreophila* on copper. Increase in initial copper concentration increases the adsorption capacity. Equilibrium isotherm shows that of the four isotherms, Temkin model is the most appropriate for explaining the

Table 3. Thermodynamic parameters for the adsorption of copper on *G. oreophila.*

ΔS(J/molK)	ΔH(kJ/mol)	ΔG(kJ/mol)				E_a(kJ/mol)
		303K	308K	313K	318K	
77.7	20.9	-2.58	-2.31	-3.42	-3.50	168.3

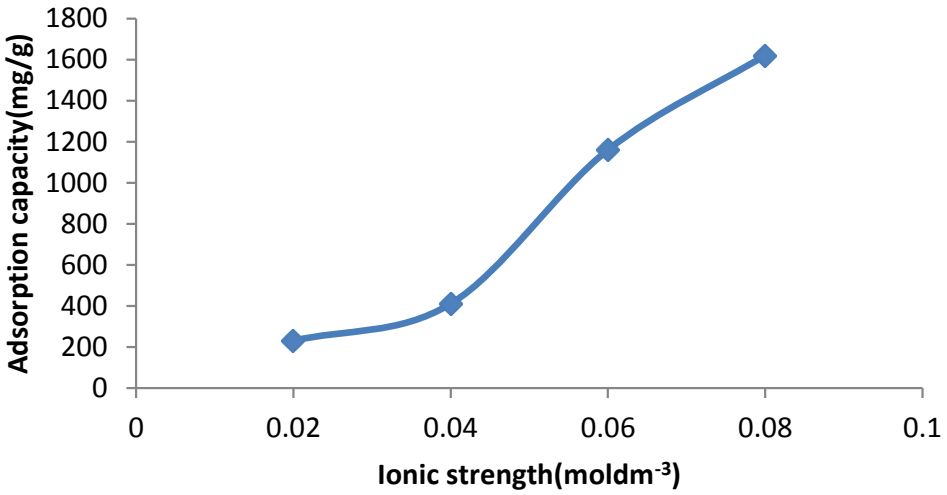

Figure 13. Impact of ionic strength on copper biosorption on *G. oreophila.*

adsorption process. D-R isotherm, as well as the activation energy, which is the minimum energy required for the adsorbent- adsorbate interaction, shows that the adsorption process is chemisorption. Increase in ionic strength significantly increased the capacity of *G. oreophila* in removing copper from solution. This study reports the usefulness of *G. oreophila* as an adsorbent for removing copper from aqueous solution.

CONFLICT OF INTERESTS

The authors have not declared any conflict of interests.

ACKNOWLEDGEMENT

The author appreciates Miss Bukola Adegeye and Dr. S. A. Ayanda for their assistance rendered in this study.

REFERENCES

Ahmada MA, Ahmada N, Bello OS (2014). Removal of Remazol Brilliant Blue Reactive Dye from Aqueous Solutions Using Watermelon Rinds as Adsorbent. Journal of Dispersion Science and Technology 36:845-858.

Ajaelu CJ, Dawodu MO, Faboro EO, Ayand OS (2017a). Copper Biosorption by Untreated and Citric Acid Modified *Senna alata* Leaf Biomass in a Batch System: Kinetics, Equilibrium and Thermodynamics Studies. Physical Chemistry 7:31-41.

Ajaelu CJ, Ibironke L, Oladinni AB (2017b). Copper (II) ions adsorption by Untreated and Chemically Modified *Tectona grandis* (Teak bark): Kinetics, Equilibrium and thermodynamic Studies. African Journal of Biotechnology 18(14):296-306.

Ajmal M, Khan AH, Ahmad S, Ahmad A (1998). Role of sawdust in the removal of copper (II) from industrial wastes. Water Research 32(10):3085-3091.

Alao O, Ajaelu CJ, Ayeni O (2014). Kinetics, Equilibrium and Thermodynamic Studies of the Adsorption of Zinc (II) ions on *Carica papaya* root powder. Research Journal of Chemical Sciences 4(11):32-38.

Atkins P, Paula J (2006) The extent of adsorption. Atkin's Physical Chemistry. 8th Ed.:916-918.

Baccar R, Blánquez P, Bouzid J, Feki M, Attiya H, Sarrà (2013). Modeling of adsorption isotherms and kinetics of a tannery dye onto an activated carbon prepared from an agricultural by-product. Fuel Processing Technology 106:408-415.

Borrok DM, Fein JB (2005). The impact of ionic strength on the adsorption of protons, Pb, Cd and Sr onto the surface of Gram negative bacteria: testing non-electrostatic, diffuse and triple-layer models. Journal of Colloid and Interface Science 286(1):10-126.

Chowdhury S, Saha PD (2012). Batch and continuous (fixed bed column) biosorption of Cu (II) by *Tamarindus indica* fruit shell, Korean Journal of Chemical Engineering 30:369-378.

Faboro EO, Olawuni IJ, Akinpelu BA, Oyedapo OO, Iwalewa EO, Obafemi CA (2018). *In Vitro* Evaluation of Antioxidant and Anti-inflammatory Properties of Methanol and Dichloromethane Extracts of the Leaf of *Globimetula oreophila.* Chemical Science International Journal 23:1-15.

Health Canada (1992). Copper. In: Guidelines for Canadian drinking water quality. Supporting documentation. Ottawa, Ontario.

International Programme on Chemical Safety (IPCS) (1998). *Copper*. Geneva, World Health Organization, International Programme on Chemical Safety (Environmental Health Criteria 200).

Larous S, Meniai AH, Lehocine MB (2005). Experimental study of the removal of copper from aqueous solutions by adsorption using

sawdust, Desalination 185(1-3):483-490.
Temkin MI (1941). Adsorption equilibrium and the kinetics of processes on nonhomogeneous surfaces and in the interaction between adsorbed molecules. Zh. Fiz. Chim 15:296-332.
Tong TS, Kassim MJ, Azraa A (2011). Adsorption of copper ion from its aqueous solution by a novel biosorbent. *Uncaria gambir*: Equilibrium, kinetics, and thermodynamic studies. Chemical Engineering Journal 170:145-153.
US EPA (1991). Maximum contaminant level goals and national primary drinking water regulations for lead and copper; final rule. US Environmental Protection Agency. Federal Register 56(110):26460-26564.
US NRC (2000). Copper in drinking water. Washington, DC, National Research Council, National Academy Press.
Wang XS, Qin Y (2005). Equilibrium Sorption Isotherms for Cu^{2+} on Rice Bran. Process Biochemistry 40:677-680.
Weber TW, Chakkravort RK (1974). Pore and solid diffusion models for fixed bed adsorbers. American Institute of Chemical Engineering Journal 20:228.
World Health Organization (WHO) (2004). Copper in water. Background document for development of WHO Guidelines for Drinking-water Quality WHO/SDE/WSH/03.04/88. https://www.who.int/water_sanitation_health/dwq/chemicals/copper.pdf
Zafar MN, Nadeem R, Hanif MA (2006). Biosorption of nickel from protonated rice bran. Journal of Harzadous Material 143:478-485.
Zhu SZ, Wang LP, Chen W (2009). Removal of Cu (II) from aqueous solution by agricultural by product: peanut hull, Journal of. Hazardous Materials 168:739-746.

Related Journals: